Article

Cell Reports

A Two-Cell Model for IL-1β Release Mediated by Death-Receptor Signaling

Graphical Abstract

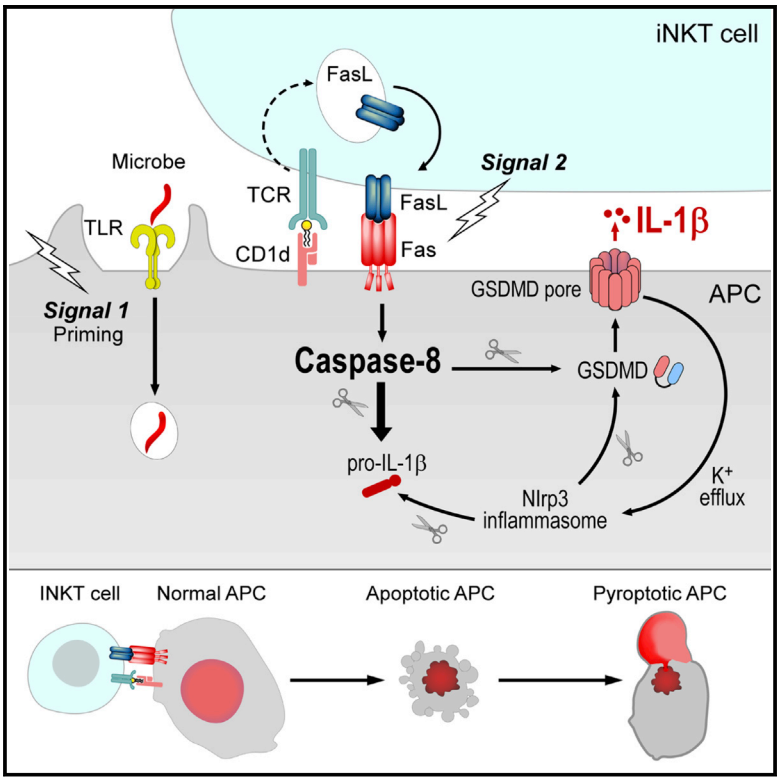

Highlights

- Infected APCs may fail to activate the inflammasome and release IL-1β
- A second cell (e.g., iNKT cell) can employ FasL to rescue IL-1β production by APCs
- Caspase-8 is the main driver of IL-1β release downstream of Fas ligation
- Caspase-8 directly cleaves GSDMD, converting apoptosis to pyroptosis

Authors

Carlos A. Donado, Anh B. Cao, Daimon P. Simmons, Ben A. Croker, Patrick J. Brennan, Michael B. Brenner

Correspondence

pbrennan3@bwh.harvard.edu (P.J.B.), mbrenner@research.bwh.harvard.edu (M.B.B.)

In Brief

How the immune system triggers IL-1β release during infection with inflammasome-evasive microbes is largely unknown. Donado et al. describe an alternative, caspase-8-dependent IL-1β secretion pathway where a second cell, the invariant natural killer T (iNKT) cell, can provide antigen-presenting cells with cell-extrinsic IL-1β release signals through FasL.

Donado et al., 2020, Cell Reports *31*, 107466
April 7, 2020
https://doi.org/10.1016/j.celrep.2020.03.030

CellPress

Cell Reports
Article

A Two-Cell Model for IL-1β Release Mediated by Death-Receptor Signaling

Carlos A. Donado,[1,2] Anh B. Cao,[2] Daimon P. Simmons,[3] Ben A. Croker,[4,5,6] Patrick J. Brennan,[7,8,*] and Michael B. Brenner[1,8,9,*]

[1]Division of Rheumatology, Inflammation and Immunity, Brigham and Women's Hospital and Harvard Medical School, Boston, MA 02115, USA
[2]Division of Medical Sciences, Harvard Medical School, Boston, MA 02115, USA
[3]Department of Pathology, Brigham and Women's and Harvard Medical School, Boston, MA 02115, USA
[4]Division of Hematology/Oncology, Boston Children's Hospital, Boston, MA 02115, USA
[5]Department of Pediatrics, Harvard Medical School, Boston, MA 02115, USA
[6]Division of Allergy, Immunology & Rheumatology, Department of Pediatrics, School of Medicine, University of California, San Diego, 9500 Gilman Drive, La Jolla, CA 92093, USA
[7]Division of Allergy and Clinical Immunology, Brigham and Women's Hospital and Harvard Medical School, Boston, MA 02115, USA
[8]Senior author
[9]Lead Contact
*Correspondence: pbrennan3@bwh.harvard.edu (P.J.B.), mbrenner@research.bwh.harvard.edu (M.B.B.)
https://doi.org/10.1016/j.celrep.2020.03.030

SUMMARY

Interleukin-1β (IL-1β) is a key orchestrator of anti-microbial immunity whose secretion is typically dependent on activation of inflammasomes. However, many pathogens have evolved strategies to evade inflammasome activation. Here we describe an alternative, two-cell model for IL-1β release where invariant natural killer T (iNKT) cells use the death receptor pathway to instruct antigen-presenting cells to secrete IL-1β. Following cognate interactions with TLR-primed bone marrow-derived dendritic cells (BMDCs), iNKT cells rapidly translocate intracellular Fas ligand to the surface to engage Fas on BMDCs. Fas ligation activates a caspase-8-dependent signaling cascade in BMDCs that drives IL-1β release largely independent of inflammasomes. The apoptotic program initiated by Fas ligation rapidly transitions into a pyroptosis-like form of cell death mediated by gasdermin D. Together, our findings support a two-cell model for IL-1β secretion that may supersede inflammasome activation when cytosolic triggers fail.

INTRODUCTION

Interleukin-1β (IL-1β) is a central mediator of inflammation that orchestrates essential immune responses against microbial invaders. It elicits widespread local and systemic effects that are intended to culminate in pathogen elimination, including leukocyte recruitment and activation, production of acute-phase reactants, and induction of fever (Dinarello, 2011). IL-1β is synthesized as an immature cytosolic precursor that requires cleavage to become biologically active. Its processing and secretion are largely regulated by inflammasomes, cytosolic multiprotein complexes that assemble following detection of microbial products, endogenous danger signals, or perturbations of cellular homeostasis in the cytosol of host cells (Latz et al., 2013; Martinon et al., 2002; Schroder and Tschopp, 2010). Most inflammasomes consist of a cytosolic sensor, the adaptor protein apoptosis-associated speck-like protein containing a caspase recruitment domain (ASC), and the effector protease caspase-1. Following inflammasome assembly, active caspase-1 catalyzes proteolytic maturation of the leaderless pro-inflammatory cytokine IL-1β and the related IL-1 family member IL-18 (Broz and Dixit, 2016; Latz et al., 2013; Schroder and Tschopp, 2010). In addition, caspase-1 cleaves the pore-forming protein gasdermin D (GSDMD), generating an N-terminal fragment that forms pores in the plasma membrane (Broz and Dixit, 2016; Kayagaki et al., 2015; Shi et al., 2015). Although these pores can serve as conduits for the release of mature IL-1β (Evavold et al., 2018; Heilig et al., 2018; Kayagaki et al., 2015; Shi et al., 2015), they also trigger pyroptosis, a lytic form of cell death characterized by cell swelling, membrane rupture, and release of soluble cytosolic contents (Aglietti et al., 2016; Ding et al., 2016; Kayagaki et al., 2015; Liu et al., 2016; Sborgi et al., 2016; Shi et al., 2015).

Inflammasome activation is controlled by two signals. The first signal, termed priming, generally induces expression of an inflammasome sensor and the substrate pro-IL-1β. The priming signal can be provided through stimulation of various Toll-like receptors (TLRs) or by the cytokine tumor necrosis factor (TNF). This first step is necessary to render the cell responsive to a second signal, which can come in the form of diverse microbial, endogenous, and environmental stimuli that trigger inflammasome assembly and activation (Broz and Dixit, 2016; Latz et al., 2013; Schroder and Tschopp, 2010). Because of their cytosolic residence, inflammasome sensors are poised to detect the presence of invasive microbes that perturb the host cell cytosol. However, many pathogens have evolved strategies to inhibit or evade the inflammasomes. Microbial invaders can do this by repressing or structurally modifying ligands or by directly inhibiting inflammasome activation through specific virulence factors (Higa et al., 2013; Maltez and Miao, 2016; Shin and

Brodsky, 2015; Stewart and Cookson, 2016; Ulland et al., 2015). Here we asked whether alternative mechanisms beyond inflammasome activation may mediate the processing and secretion of IL-1β during conditions where cell-intrinsic recognition of cytosolic triggers of inflammasomes is compromised.

Invariant natural killer T (iNKT) cells are innate T cells that play a major role in host defense against bacterial, fungal, and viral infections. They exist in a poised effector state that allows them to respond in synchrony with the innate immune response, performing distinct effector functions significantly more rapidly than adaptive, major histocompatibility complex (MHC)-restricted T cells. iNKT cells express evolutionarily conserved, semi-invariant αβ T cell receptors (TCRs) responsive to endogenous and microbial lipid antigens bound to the non-polymorphic, class I-like molecule CD1d. One of the functional hallmarks of iNKT cells is their remarkable ability to catalyze immune responses in large part by rapidly transactivating other leukocytes through cytokine production and contact-dependent mechanisms (Brennan et al., 2013). Given their role as cellular adjuvants during the early stages of infection, we hypothesized that iNKT cells might contribute to the production of IL-1β by antigen-presenting cells (APCs) and that this may be important in the recognition of pathogens that evade inflammasome activation from within the cytosol of host cells.

Here we describe a two-cell model for IL-1β release where iNKT cells instruct TLR-primed bone marrow-derived dendritic cells (BMDCs) to secrete IL-1β. Following cognate, CD1d-dependent recognition of primed BMDCs, we found that iNKT cells rapidly translocate pre-existing intracellular Fas ligand (FasL) to their surface and engage Fas on BMDCs. Fas ligation resulted in limited activation of the Nlrp3 inflammasome in BMDCs, but most of the IL-1β was released in an inflammasome-independent manner via caspase-8. Although Fas engagement initiated the apoptotic program in BMDCs, cells quickly transitioned to pyroptosis in a manner that was dependent on the pore-forming protein GSDMD. Importantly, we show that iNKT cells can employ FasL to elicit IL-1β release by BMDCs infected with the commensal microbe *Bacteroides fragilis* (*B. fragilis*) and the obligate intracellular pathogen *Chlamydia trachomatis* (*C. trachomatis*) under conditions where these organisms fail to activate inflammasomes in a cell-intrinsic manner. Thus, iNKT cells are poised to deliver IL-1β-secretion signals through FasL, and this two-cell mechanism for IL-1β release may be important against microbes that fail to activate the inflammasomes from within the host cell cytosol.

RESULTS

iNKT Cells Induce IL-1β Secretion by BMDCs through Cognate Interactions

Bi-directional cross-talk with APCs is central to the ability of iNKT cells to enhance immunity (Brennan et al., 2013). Thus, we hypothesized that iNKT cells might promote IL-1β release from APCs. To assess whether iNKT cells could trigger the release of IL-1β, we co-cultured iNKT cells with BMDCs that had been primed with the TLR2 agonist Pam3CSK4 (P3C). Although a priming signal alone proved to be insufficient to elicit secretion of IL-1β by BMDCs, addition of iNKT cells to P3C-primed BMDCs led to a significant release of IL-1β. Indeed, iNKT-driven IL-1β release was comparable to that induced by the Nlrp3 inflammasome activator monosodium urate (MSU) (Figure 1A). When P3C-primed BMDCs were loaded with a strong synthetic lipid agonist for the iNKT cell TCR, α-galactosylceramide (αGalCer), even higher levels of IL-1β were released (Figure 1B). Co-culture with iNKT cells resulted in accumulation of extracellular IL-1β over time (Figure 1C), suggesting that they induce gradual rather than the rapid, all-or-none release of IL-1β induced by the canonical Nlrp3 inflammasome agonist nigericin. Immunoblotting showed that iNKT cells induced secretion of the processed form of IL-1β by P3C-primed BMDCs, and its release coincided with depletion of intracellular pro-IL-1β (Figure 1D). To determine whether the release of IL-1β was dependent on cognate recognition of the lipid antigen-presenting molecule CD1d by iNKT cells, we used BMDCs from CD1d-deficient mice. Strikingly, co-culture of iNKT cells with P3C-primed BMDCs from mice deficient in CD1d resulted in the complete absence of extracellular IL-1β, whereas the ability of nigericin to elicit this cytokine was unaffected in CD1d-deficient BMDCs (Figure 1E). Together, these results demonstrate that cognate interactions between iNKT cells and BMDCs, whether in the presence of self or foreign lipid antigens, are sufficient to drive IL-1β release by TLR-primed BMDCs.

iNKT Cells Employ the Death Receptor Ligand FasL to Elicit IL-1β Release by TLR-Primed BMDCs

We next sought to determine the mechanism by which iNKT cells induced IL-1β release by BMDCs. We failed to detect secreted IL-1β when P3C-primed BMDCs were cultured with the cell-free supernatant of TCR-activated iNKT cells (Figure 2A), suggesting that iNKT cells employ a cell-surface molecule, rather than a soluble factor, to elicit IL-1β release. Based on how rapidly iNKT cells induced TLR-primed BMDCs to secrete IL-1β (Figures 1C and 1D), we reasoned that iNKT cells were likely to express the relevant molecule at resting state as part of their "innate-like" phenotype (Cohen et al., 2013; Kim et al., 2015). To identify a candidate molecule, we queried the ImmGen database (Heng et al., 2008) and compared the expression of all cell-surface molecules between iNKT cells and other αβ T cells. One of the most highly and differentially expressed surface molecules we found in iNKT cells was *Fasl* (Figure 2B). To determine whether iNKT cells employ FasL to elicit IL-1β release by BMDCs, we co-cultured iNKT cells and P3C-primed BMDCs in the presence of a FasL-blocking antibody (Figure 2C). Strikingly, FasL-blockade completely abrogated the ability of iNKT cells to induce IL-1β secretion by BMDCs. As observed with FasL blockade, iNKT cells were unable to elicit IL-1β release by Fas-deficient BMDCs (Figure 2D). Together, these results suggest that iNKT cells employ the death receptor ligand FasL to instruct TLR-primed BMDCs to secrete IL-1β.

GM-CSF-derived bone marrow cultures, widely referred to as BMDCs, serve as useful model APCs and consist of a heterogeneous population of monocyte-derived macrophages and conventional DC-like cells (Helft et al., 2015). It has been shown recently that monocyte-derived macrophages, the most abundant cell population found in GM-CSF-derived BM cultures,

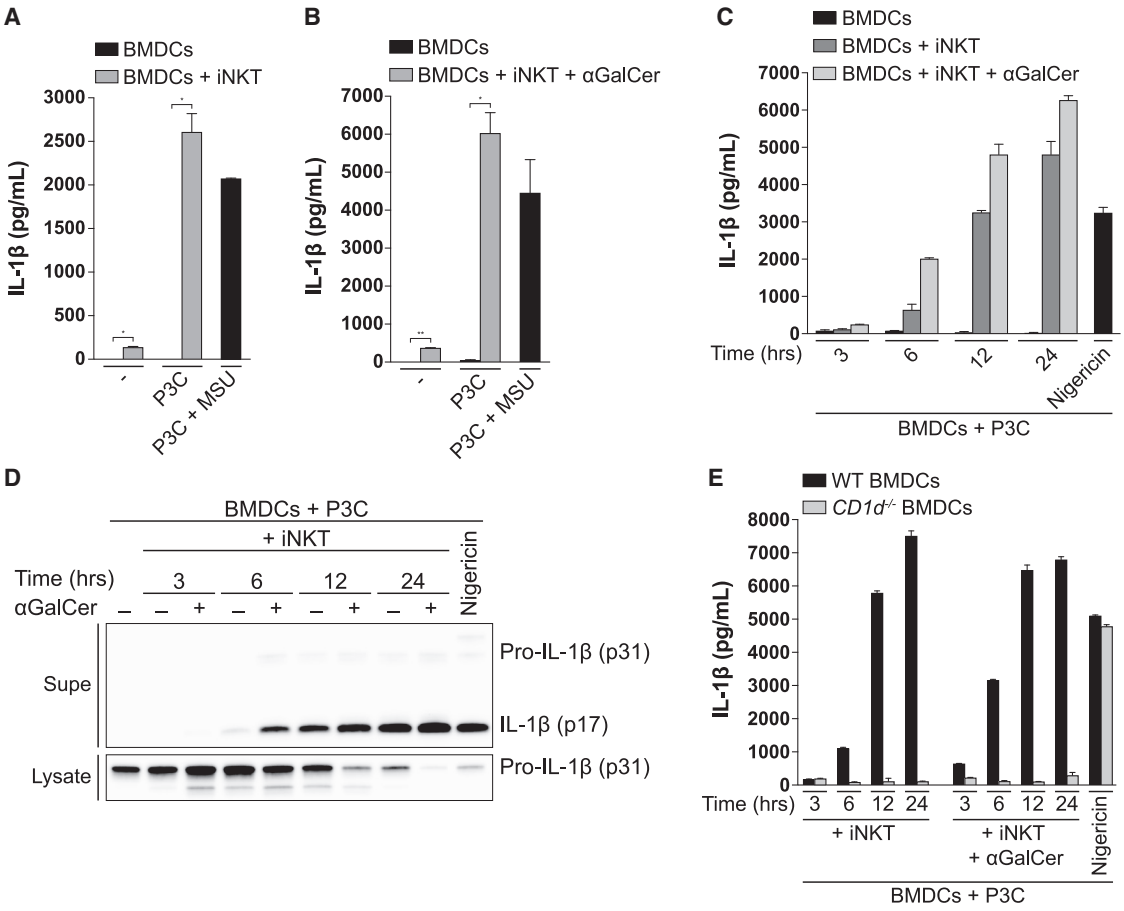

Figure 1. iNKT Cells Induce IL-1β Secretion by BMDCs in a CD1d-Dependent Manner

(A and B) BMDCs were left unprimed or primed with Pam3CSK4 (P3C; 0.5 μg/mL) for 24 h and subsequently co-cultured with iNKT cells for 24 h in the (A) absence or (B) presence of αGalCer (50 ng/mL). IL-1β release was quantified by ELISA. As a control, BMDCs were primed with P3C for 4 h, followed by 6-h stimulation with MSU (100 μg/mL). The same concentrations of P3C, αGalCer, and MSU were used throughout all experiments.

(C and D) P3C-primed BMDCs were cultured alone or with iNKT cells for the indicated times in the presence or absence of αGalCer. IL-1β release was quantified by ELISA (C), and cell-associated and extracellular IL-1β were analyzed by immunoblot (D). As a control, BMDCs were primed with P3C for 4 h, followed by 1-h stimulation with nigericin (10 μM).

(E) P3C-primed BMDCs from WT and *CD1d*$^{-/-}$ mice were co-cultured with iNKT cells for the indicated times in the absence or presence of αGalCer. IL-1β release was quantified by ELISA. P3C-primed BMDCs stimulated with nigericin were used as a control.

Error bars represent mean + SD of triplicate samples. Each panel is representative of at least three different experiments. *$p < 0.05$, **$p < 0.01$, as determined by Student's unpaired t test. Supe, supernatant.

are the cellular source of IL-1β following classical inflammasome activation in these cultures (Erlich et al., 2019). To identify which cell type secretes IL-1β in response to Fas ligation, we sorted monocyte-derived macrophages (MDMs; CD11c^{+}CD11b^{hi} MHC-II^{lo-int}CD115^{+}MerTK^{+}) and DCs (GM-DCs; CD11c^{+} CD11b^{int}MHC-II^{high}CD115^{-}CD135^{+}) from GM-CSF-derived BM cultures using fluorescence-activated cell sorting (FACS) and stimulated them with recombinant hexameric FasL (rFasL) (Holler et al., 2003) after priming with P3C. In agreement with a prior report studying inflammasome activation (Erlich et al., 2019), we found that, within BMDC cultures, MDMs, but not GM-DCs, were responsible for IL-1β secretion following stimulation with rFasL or the Nlrp3 inflammasome agonist MSU (Figures S1A and S1B). It is likely that the inability of GM-DCs to secrete IL-1β in response to Fas ligation is due to their lack of expression of inflammasome components and pro-IL-1β, as reported previously (Erlich et al., 2019).

We next investigated the kinetics of FasL expression on the surface of iNKT cells. Although iNKT cells lacked detectable FasL on their surface, they expressed a large pool of intracellular FasL at steady state (Figure 2E). iNKT cells rapidly mobilized intracellular FasL to their surface upon co-culture with BMDCs, and this translocation was entirely dependent on CD1d (Figure 2F). The stronger TCR stimulus provided by αGalCer elicited even more rapid and pronounced expression of surface FasL by iNKT cells (Figure 2F). These data suggest that iNKT cells constitutively express intracellular FasL stores that are rapidly translocated to the surface upon engagement of their TCRs. iNKT cells are thus poised to engage Fas on TLR-primed BMDCs

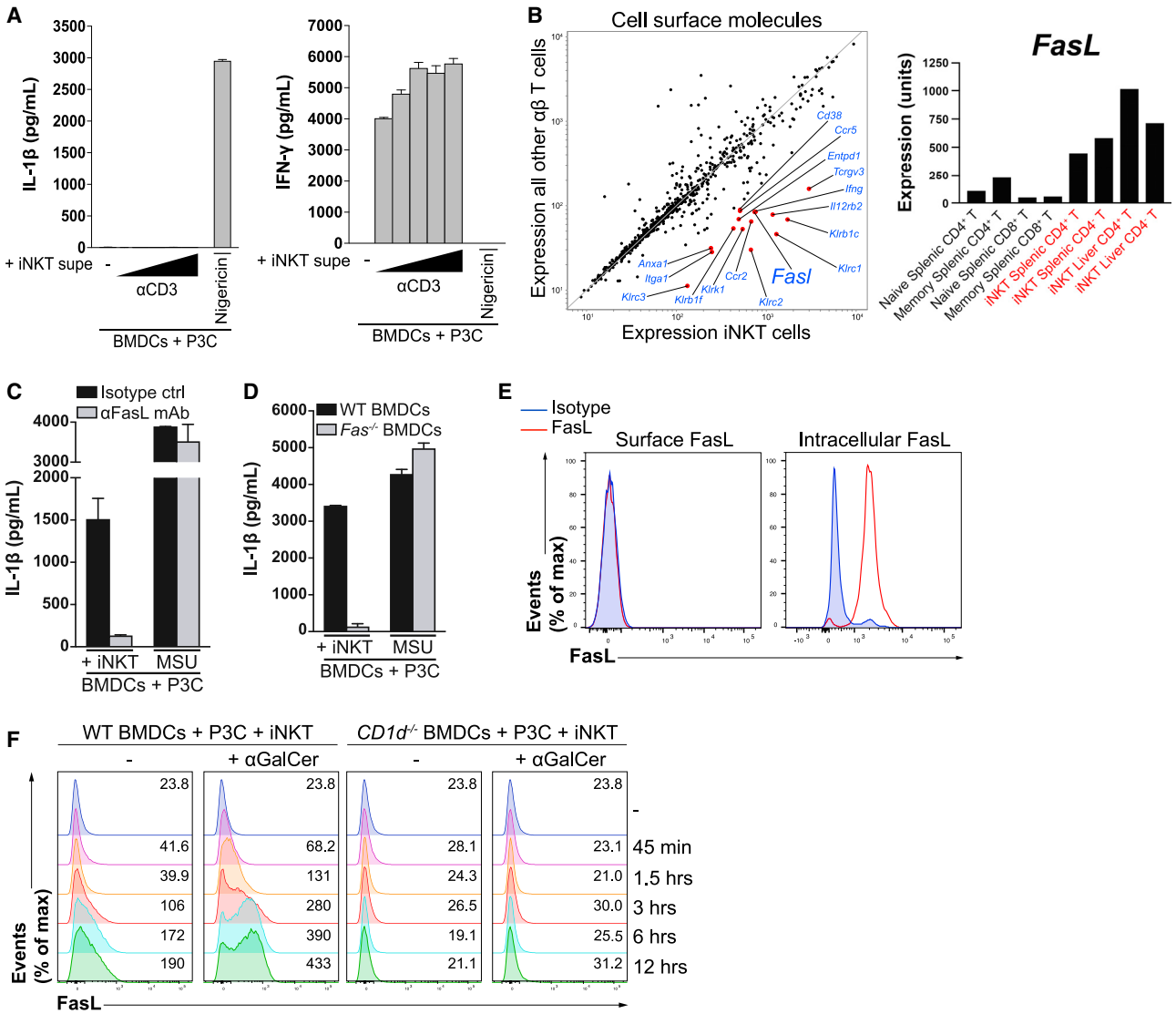

Figure 2. iNKT Cells Employ the Death Receptor Ligand FasL to Instruct TLR-Primed BMDCs to Release IL-1β

(A) iNKT cells were cultured in the presence of increasing concentrations of plate-bound anti-CD3 for 24 h, after which their cell-free Supes were used to stimulate P3C-primed BMDCs for 24 h. IL-1β (left) and interferon γ (IFN-γ; right) in the Supes were quantified by ELISA. Nigericin-stimulated BMDCs were used as a control.

(B) The ImmGen database was mined to compare the expression of cell-surface proteins (Gene Ontology term "cell surface," GO0009986) expressed by iNKT cells versus other αβ T cells. The red dots represent genes expressed by iNKT cells with a fold change of greater than 5 compared with all other αβ T cells. Expression values comparing class means for specific T cell populations are shown in the right panel.

(C) P3C-primed BMDCs were co-cultured with iNKT cells for 24 h in the presence of a FasL-blocking antibody (αFasL mAb) or an isotype control. IL-1β release was quantified by ELISA. MSU-treated BMDCs were used as a control.

(D) P3C-primed BMDCs from WT and *Fas*$^{-/-}$ mice were co-cultured with iNKT cells for 24 h. IL-1β release was quantified by ELISA. MSU-treated BMDCs were used as a control.

(E) Resting iNKT cells were stained with a FasL-specific antibody or an isotype control and subsequently analyzed by flow cytometry. The left panel represents surface staining, whereas the right panel represents permeabilized iNKT cells.

(F) P3C-primed BMDCs from WT and *CD1d*$^{-/-}$ mice were co-cultured with CellTrace Violet-labeled-iNKT cells for the indicated times in the presence or absence of αGalCer, and the expression of FasL on the surface of iNKT cells was analyzed by flow cytometry. Numbers on the right of each histogram represent mean fluorescence intensity values.

Error bars represent mean + SD of triplicate samples. Each panel is representative of at least three different experiments.

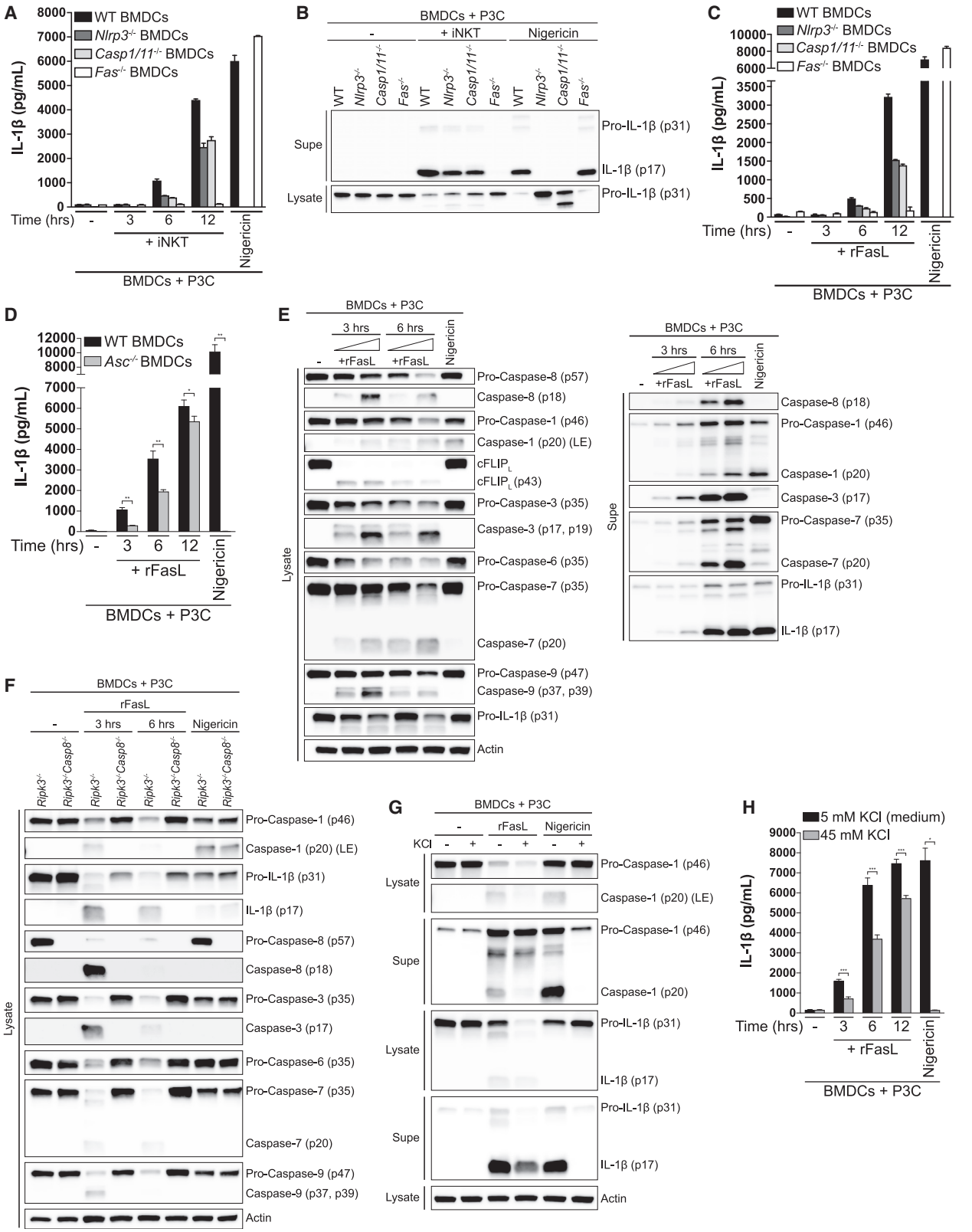

(legend on next page)

following cognate interactions, resulting in release of bioactive IL-1β.

Fas Ligation Triggers Inflammasome-Dependent and -Independent IL-1β Release via Caspase-8

Having demonstrated that iNKT cells employ FasL to transactivate an IL-1β secretion pathway in BMDCs, we next sought to determine the relevant signaling pathways downstream of Fas ligation. Among inflammasome sensors, Nlrp3 is the most promiscuous, being activated by a diverse array of stimuli ranging from microbial and sterile molecules to disturbances in cytosolic homeostasis (Broz and Dixit, 2016; Latz et al., 2013; Schroder and Tschopp, 2010; Swanson et al., 2019). Co-culture of iNKT cells with either Nlrp3- or caspase-1/11-deficient BMDCs resulted in a partial reduction in IL-1β release as detected by ELISA (Figure 3A) and immunoblot (Figure 3B). Although IL-1β release fell by approximately 50% at early time points, there was little effect on release of IL-1β over time (Figure S2A). Further, the partial dependence on the Nlrp3 inflammasome was similar in magnitude when αGalCer was added to the co-culture (Figures S2B and S2C), confirming that presentation of self or foreign lipid antigens results in activation of phenotypically equivalent pathways. We also failed to detect the active p20 subunit of caspase-1 in Nlrp3-deficient BMDCs, confirming that the Nlrp3 inflammasome is activated in response to Fas ligation (Figure S2D). These results suggest that, although iNKT cells can transactivate the Nlrp3 inflammasome in BMDCs, they also elicit activation of an inflammasome-independent pathway that has a larger contribution to IL-1β release.

To further investigate the molecular events that occur downstream of Fas ligation in BMDCs, we used rFasL (Holler et al., 2003). The addition of rFasL to P3C-primed BMDCs resulted in robust release of IL-1β that was qualitatively equivalent to that induced by iNKT cells (Figure 3C). We also detected the active, cleaved form of caspase-1 in the supernatants of TLR-primed BMDCs treated with rFasL (Figure 3E), indicating that, like iNKT cells, rFasL was able to induce inflammasome activation. Further, we observed a similar reduction in IL-1β release in ASC-deficient BMDCs compared with wild-type (WT) BMDCs (Figure 3D), as observed in Nlrp3- and caspase-1/11-deficient BMDCs (Figure 3C).

Fas ligation elicits formation of a death-inducing signaling complex (DISC) that includes the adaptor protein Fas-associated death domain (FADD) and caspase-8, the initiator caspase of the extrinsic apoptotic pathway. Engagement of Fas triggers recruitment of FADD to the intracellular region of Fas, allowing caspase-8 to bind to Fas-associated FADD. This results in recruitment of additional caspase-8 molecules, leading to caspase-8 oligomerization and subsequent self-cleavage-induced activation. Active caspase-8 in turn cleaves and activates the executioner caspases-3, -6, and -7, which go on to cleave a number of substrates to drive the cellular changes characteristic of apoptosis (Green and Llambi, 2015; Strasser et al., 2009). As expected, addition of rFasL to P3C-primed BMDCs resulted in robust cleavage of caspase-8 into the active p18 fragment (Figure 3E). Likewise, Fas ligation also resulted in cleavage of the executioner caspases-3, -6, and -7 into their active forms (Figure 3E).

Next we tested whether caspase-8 is required for FasL-induced IL-1β cleavage by BMDCs. Genetic ablation of *caspase-8* results in embryonic lethality in mice because of uncontrolled necroptosis, a form of programmed necrosis that requires the kinase activity of receptor-interacting protein kinases 1 and 3 (RIPK1 and RIPK3, respectively) and is executed by the pseudokinase mixed lineage kinase-like (MLKL) (Galluzzi et al., 2017; Silke et al., 2015). Thus, to find out whether caspase-8 is required for FasL-induced IL-1β processing, we assessed the effect of loss of caspase-8 in *Ripk3*-deficient BMDCs. Before doing so, we confirmed that RIPK3 and MLKL are not required for IL-1β release following Fas crosslinking (Figure S3A). Caspase-8-deficient BMDCs were unable to process IL-1β following Fas ligation (Figure 3F). Further, in the absence of caspase-8, we failed to detect the active, cleaved forms of caspase-1; the executioner caspase-3, -6, and -7; and caspase-9, the initiator caspase of the intrinsic apoptotic pathway (Figure 3F). Thus, caspase-8 orchestrates the major events occurring downstream of Fas ligation; it directly cleaves the majority of pro-IL-1β, amplifies its processing and release by driving activation of the Nlrp3 inflammasome, and triggers activation of all pro-apoptotic caspases.

We next asked whether potassium efflux, a common trigger of the Nlrp3 inflammasome (Muñoz-Planillo et al., 2013), drives inflammasome activation downstream of Fas ligation. Consistent with published data, nigericin-driven caspase-1 cleavage and IL-1β processing and release were completely inhibited when potassium efflux was blocked (Figure 3G). In contrast, although raising the concentration of extracellular potassium completely inhibited FasL-induced caspase-1 processing (Figure 3G), it only partially blocked IL-1β cleavage and secretion (Figures 3G and 3H). The reduction in IL-1β release was similar to that observed in

Figure 3. Fas Ligation Triggers Inflammasome-Dependent and Independent IL-1β Release via Caspase-8

(A and B) P3C-primed BMDCs from WT, *Nlrp3*$^{-/-}$, *Caspase1/11*$^{-/-}$ and *Fas*$^{-/-}$ mice were cultured alone or with iNKT cells for (A) the indicated times or (B) 12 h. IL-1β release was quantified by ELISA (A) and cell-associated (lysate) and extracellular (Supe) IL-1β were analyzed by immunoblot (B). Nigericin-treated BMDCs were used as a control.

(C and D) P3C-primed BMDCs from (C) WT, *Nlrp3*$^{-/-}$, *Caspase1/11*$^{-/-}$, and *Fas*$^{-/-}$ or (D) WT and *Asc*$^{-/-}$ mice were cultured alone or in the presence of recombinant, hexameric FasL (rFasL) for the indicated times. IL-1β release was quantified by ELISA.

(E) P3C-primed BMDCs were cultured in the presence of increasing concentrations of rFasL for the indicated times, and the cell lysates (left) and cell-free Supes (right) were probed for the indicated proteins by immunoblot.

(F) P3C-primed BMDCs from *Ripk3*$^{-/-}$ and *Ripk3*$^{-/-}$*Caspase-8*$^{-/-}$ mice were cultured in the presence of rFasL for the indicated times, and the cell lysates were probed for the indicated proteins by immunoblot.

(G and H) P3C-primed BMDCs were treated with rFasL in the presence or absence of 45 mM KCl for (G) 6 h or (H) the indicated times. The cell lysates and cell-free Supes were probed for the indicated proteins by immunoblot (G) and IL-1β release was quantified by ELISA (H).

Error bars represent mean + SD of triplicate samples. Each panel is representative of at least three different experiments. *$p < 0.05$, **$p < 0.01$, ***$p < 0.001$, as determined by Student's unpaired t test. LE, long exposure. See also Figures S2 and S3.

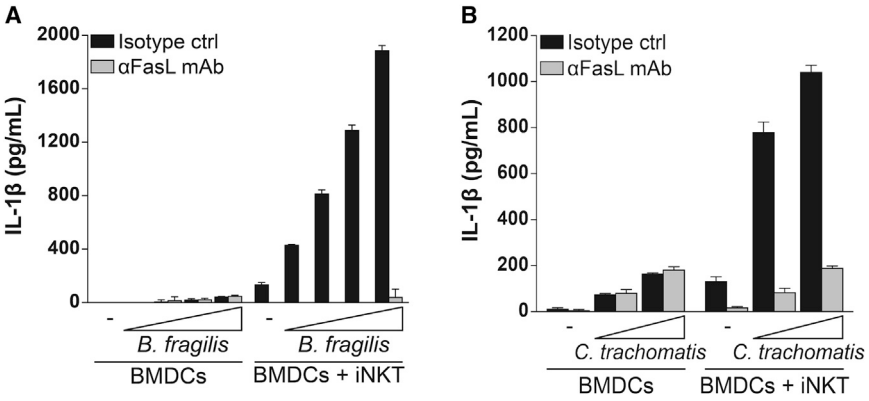

Figure 4. iNKT Cells Induce IL-1β Secretion by BMDCs during Infection with Microbes that Fail to Elicit Strong IL-1β Release in a Cell-Intrinsic Manner

BMDCs were infected with (A) *B. fragilis* or (B) *C. trachomatis* at increasing MOIs, washed, and cultured alone or with iNKT cells for 24 h in the presence of a FasL-blocking antibody (αFasL mAb) or an isotype control. IL-1β release was quantified by ELISA. Error bars represent mean + SD of triplicate samples; panels are representative of three and two independent experiments, respectively.

inflammasome-deficient BMDCs stimulated with rFasL (Figures 3C and 3D). Thus, Fas ligation appears to induce potassium efflux via caspase-8 to trigger activation of the Nlrp3 inflammasome.

Caspase-8 oligomerizes at the DISC, where it can form homodimers or heterodimers with cellular FLICE/caspase-8-like inhibitory protein (cFLIP), a caspase-8-like protein that lacks proteolytic activity. Caspase-8 homodimers become catalytically active following autoproteolytic cleavage, and these active homodimers drive apoptosis downstream of death receptor ligation. On the other hand, heterodimerization with cFLIP confers enzymatic activity to the heterodimer even in the absence of proteolytic processing of caspase-8, and these caspase-8:cFLIP heterodimers inhibit necroptosis by cleaving RIPK1 and RIPK3 (Boatright et al., 2004; Green and Llambi, 2015; Oberst et al., 2011; Pop et al., 2011; Tummers and Green, 2017). Moreover, cFLIP itself is a substrate for active caspase-8, which can cleave it when engaged in homodimers or heterodimers with cFLIP (Micheau et al., 2002). We observed complete cleavage of the long isoform of cFLIP (cFLIP$_L$) into the p43 form (Figure 3E), suggesting that the entire pool of intracellular cFLIP in P3C-primed BMDCs is cleaved by caspase-8 homodimers or capase-8/cFLIP heterodimers following Fas ligation. We next asked whether proteolytic processing of caspase-8 is required for IL-1β release downstream of Fas ligation and whether this mechanism is driven by caspase-8 homodimers or caspase-8:cFLIP heterodimers. To this end, we used BMDCs from a caspase-8 mutant knockin mouse (*Casp8*$^{DA/DA}$) in which autoproteolytic processing is prevented by replacing aspartate 387 with an alanine (Philip et al., 2016). We found that BMDCs that are incapable of undergoing caspase-8 processing were significantly impaired in their ability to release IL-1β following Fas ligation by iNKT cells (Figure S3B), suggesting that FasL-induced IL-1β release requires caspase-8 self-processing and is most efficiently driven by caspase-8 homodimers. Together, our results suggest that Fas ligation deploys caspase-8 to elicit activation of inflammasome-dependent and -independent pathways for release of IL-1β.

iNKT Cells Instruct BMDCs to Secrete IL-1β following Infection with Microbes that Fail to Activate the Inflammasome

We next asked whether iNKT cells can trigger IL-1β secretion by BMDCs in situations where microbes fail to activate the inflammasome via cell-intrinsic mechanisms. The intestinal microbe *B. fragilis* has been reported to lack the ability to induce significant IL-1β secretion by macrophages in a cell-autonomous setting (Chen et al., 2016). Similarly, we found that infection with live *B. fragilis* failed to induce substantial IL-1β secretion by BMDCs (Figure 4A). In contrast, co-culture of iNKT cells with BMDCs that had been infected with *B. fragilis* resulted in a significant dose-dependent increase in the amount of secreted IL-1β. Addition of a FasL-blocking antibody to the culture completely abrogated the ability of iNKT cells to elicit secretion of IL-1β by *B. fragilis*-infected BMDCs. Next we asked whether iNKT cells could also elicit IL-1β release by BMDCs infected with the obligate intracellular pathogen *C. trachomatis*, a microorganism known to cause significant immunopathology. Although infection with *C. trachomatis* induced weak IL-1β release by BMDCs, addition of iNKT cells resulted in robust secretion of IL-1β by BMDCs (Figure 4B). As observed for *B. fragilis*, the release of IL-1β induced by iNKT cells was entirely dependent on FasL. These results suggest that iNKT cells have the capacity to fill a gap in the recognition of microbes that fail to activate the inflammasome from within the cytosol of host cells.

Fas Ligation Drives the Transition from Apoptosis to Necrosis in BMDCs

Ligation of the death receptor Fas drives extrinsic apoptosis, classically a form of non-inflammatory cell death that is morphologically and biochemically distinct from necrotic cell death pathways like pyroptosis. Some of the features of apoptotic cell death include cytoplasmic shrinkage, phosphatidylserine exposure on the outer leaflet of the plasma membrane, chromatin condensation, membrane blebbing, and formation of apoptotic bodies (Galluzzi et al., 2018; Nagata, 2018). In contrast, pyroptosis is characterized by cell swelling and plasma membrane rupture, which are dependent on formation of plasma membrane pores by members of the gasdermin family of proteins (Kovacs and Miao, 2017; Shi et al., 2017). The consequent release of intracellular contents and proinflammatory molecules defines pyroptosis as an inflammatory form of cell death. To begin to characterize cell death following co-culture of iNKT cells with P3C-primed BMDCs, we stained the cells with the phosphatidylserine-binding protein annexin V and the

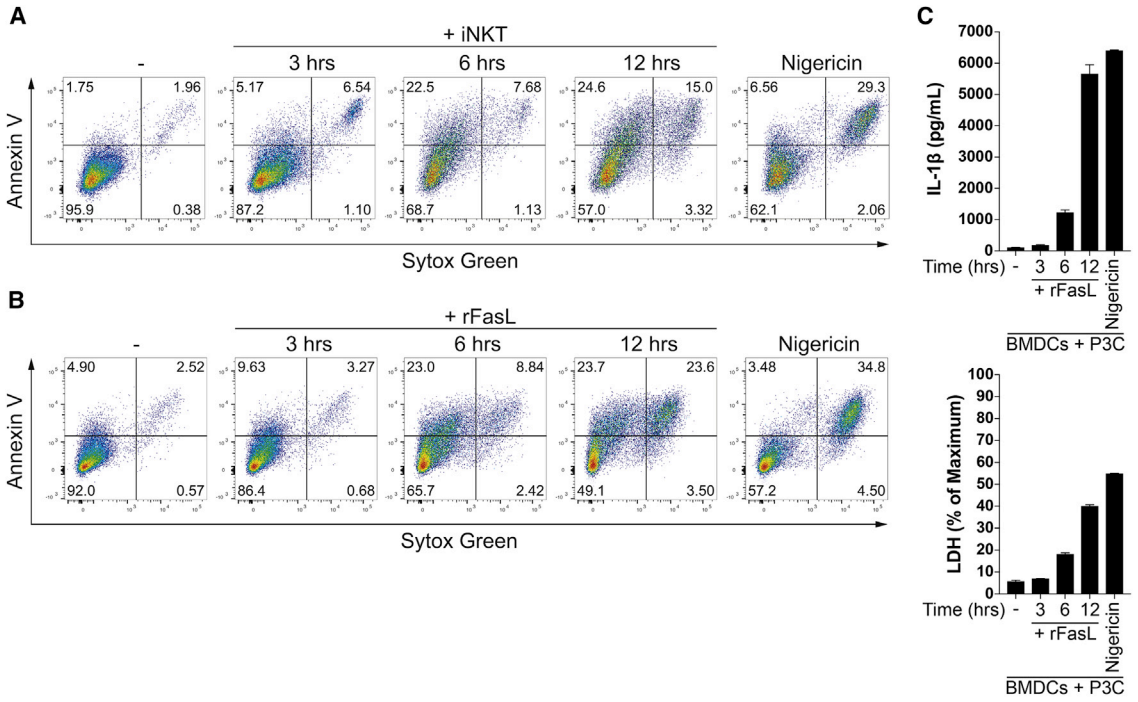

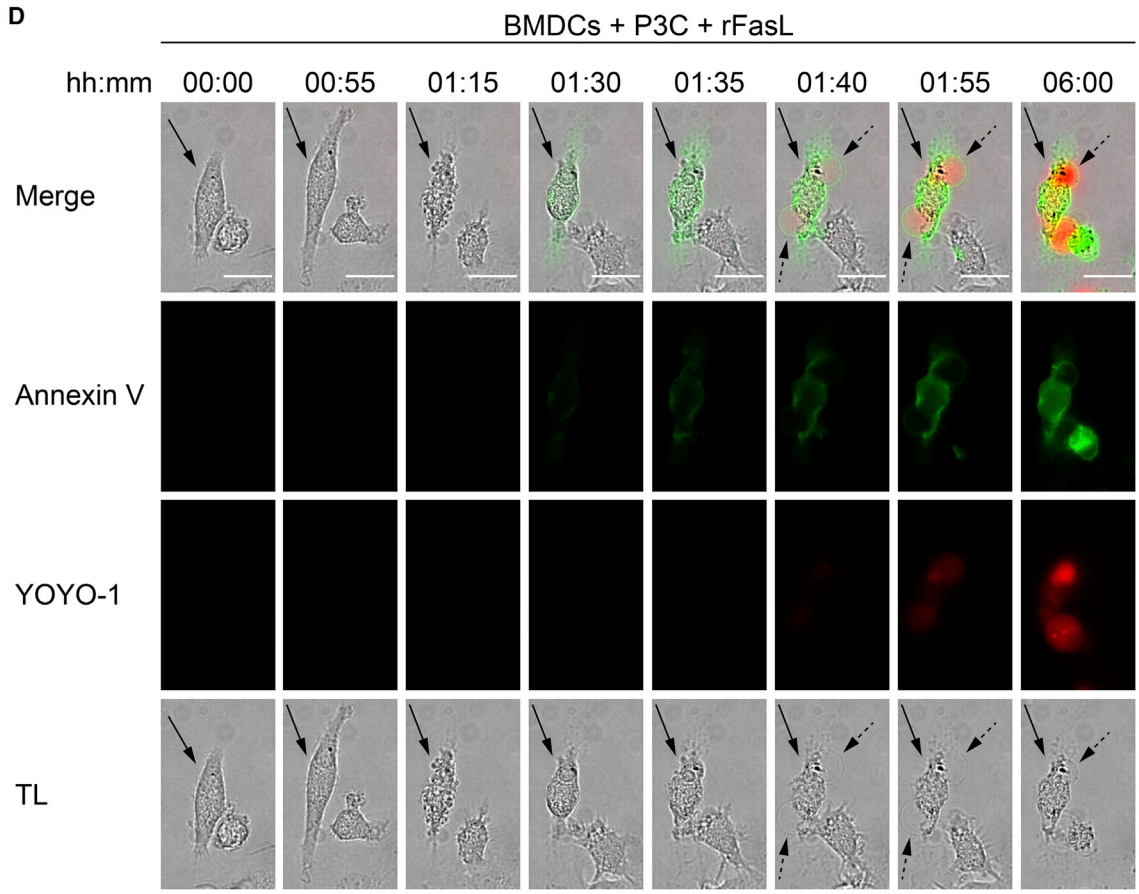

(legend on next page)

membrane-impermeant DNA-intercalating dye Sytox Green and analyzed the cells by flow cytometry. Cells that become single-positive for annexin V are considered to be undergoing early apoptosis, whereas cells that also internalize Sytox Green have become membrane permeable and are deemed necrotic. Although a fraction of BMDCs co-cultured with iNKT cells became positive only for annexin V, a substantial percentage also stained positive with Sytox Green at later time points (Figure 5A). A stronger TCR stimulus provided by αGalCer resulted in more pronounced death of BMDCs, characterized by increases in the annexin V single-positive and annexin V/Sytox Green-double positive populations (Figure S4A). Following Fas crosslinking using rFasL, P3C-primed BMDCs showed flow cytometry staining patterns comparable with those observed with iNKT cell co-culture (Figure 5B). We next measured the release of cytosolic lactate dehydrogenase (LDH) into the medium as an indication of loss of plasma membrane integrity, a feature of necrotic cell death. We detected a significant amount of LDH in the supernatants of P3C-primed BMDCs following Fas crosslinking, and the appearance of extracellular LDH correlated with the release of IL-1β (Figure 5C). Together, these results suggest that Fas ligation drives cell death that exhibits features of both apoptosis and necrosis in TLR-primed BMDCs.

We considered the possibility that apoptotic cell death and necrosis could be occurring sequentially or, alternatively, that they could occur in exclusive cell populations. To distinguish these possibilities, we used a live microscopy assay to discriminate apoptotic cells from necrotic cells based on three criteria. First, we tracked whether cells underwent shrinkage or swelling, morphological hallmarks of apoptotic and necrotic cells, respectively. Second, we evaluated whether cells externalized phosphatidylserine and, thus, bound annexin V on the outer leaflet of their plasma membrane, as expected of cells undergoing apoptosis. Third, we monitored loss of plasma membrane integrity, a feature of necrosis (Galluzzi et al., 2018), as assessed by staining with the membrane-impermeable, nucleic acid-binding dye YOYO-1. Fas ligation rapidly induced cytoplasmic shrinkage and membrane blebbing, both features of apoptosis (Figures 5D, S4B, and S4C; Videos S1 and S2). BMDCs then proceeded to stain with annexin V, and this was rapidly followed by swelling and lysis, as evidenced by formation of large plasma membrane balloons that are characteristic of necrosis. Although the majority of BMDCs exhibited a brief lag between annexin V staining and lysis (~80%), about 20% of BMDCs progressed so rapidly from an apoptotic to a necrotic morphotype that our 5-min imaging intervals failed to capture annexin V staining of the plasma membrane preceding cell lysis (Figure S4C and S4D). The lack of a substantial lag between annexin V and YOYO-1 staining suggested that BMDCs initiated but did not complete the classic apoptotic program. Further, annexin V staining was not limited to the outer leaflet of the plasma membrane. Following membrane permeabilization, annexin V increasingly stained the cytoplasm of cells, and this occurred concomitantly with incorporation of YOYO-1.

Following Fas crosslinking, we also noticed that the YOYO-1 staining spread from the nucleus to the cytoplasm and plasma membrane balloons as BMDCs adopted a pyroptotic-like morphotype (Figures 5D, S4B, S4C, S5A, and S5B). Apoptotic and pyroptotic cells have been reported to undergo chromatin condensation (pyknosis), but although the nuclei of apoptotic cells then experience membrane rupture and DNA fragmentation (karyorrhexis), the nuclei of pyroptotic cells remain intact (Galluzzi et al., 2018; Miao et al., 2011). Thus, we reasoned that classical pyroptosis is characterized by confinement of nuclear DNA in the nucleus, but if it is preceded by apoptosis, then DNA may diffuse into the cytoplasm and pyroptotic balloons. To test this hypothesis, we labeled P3C-primed BMDCs with the fluorescent, cell-permeable DNA probe silicon-rhodamine Hoechst (SiR DNA) and tracked the nuclear DNA over time. After addition of rFasL, P3C-primed BMDCs underwent substantial nuclear condensation concurrently with membrane blebbing and cytoplasmic shrinkage. When the cells transitioned to necrosis, as characterized by formation of large plasma membrane balloons and YOYO-1 staining, the nuclear DNA diffused into the cytoplasm and plasma membrane balloons (Figures 6A, 6C, S5A, and S5B; Video S3). This observation was in stark contrast to BMDCs stimulated to undergo canonical pyroptosis using nigericin (Figures 6B and 6C), where the nucleus underwent condensation but the SiR-DNA staining persisted as a single large speck over time, suggesting that the nuclear DNA remained confined to the nucleus. Thus, it is likely that fragmented nuclear DNA leaks into the cytoplasm and necrotic plasma membrane balloons when apoptosis is converted into necrosis, a feature not apparent in cells that undergo classical pyroptosis. Indeed, TUNEL staining confirmed that only BMDCs treated with rFasL, but not those stimulated with nigericin, experienced significant DNA fragmentation (Figure S5C). Together, the data suggest that Fas ligation drives the rapid transition from early apoptosis to necrosis in TLR-primed BMDCs.

Figure 5. Fas Ligation Drives the Transition from Apoptosis to Necrosis in BMDCs

(A and B) P3C-primed BMDCs were cultured alone or with (A) CellTrace Violet-labeled iNKT cells or (B) rFasL. After the indicated times, the cells were harvested, labeled with Sytox Green and annexin V, and the extent of early-apoptotic and necrotic BMDCs was analyzed by gating on CellTrace Violet-negative, CD11c-positive BMDCs. Nigericin-treated BMDCs were used as a control.

(C) P3C-primed BMDCs were cultured alone or in the presence of rFasL for the indicated times. Top: IL-1β release was quantified by ELISA. Bottom: LDH in the extracellular medium was monitored by an enzymatic assay. Nigericin-treated BMDCs were used as a control.

(D) P3C-primed BMDCs were stimulated with rFasL, and morphological changes (transmitted light, TL), annexin V (green), and YOYO-1 (red) staining were assessed by live imaging over 6 h. Images were captured every 5 min, and representative time points are shown. The arrow indicates a representative cell. Dotted arrows point at necrotic plasma membrane balloons. The scale bars represent 10 μm.

Error bars represent mean + SD of triplicate samples. Each panel is representative of at least three different experiments. See also Figure S4.

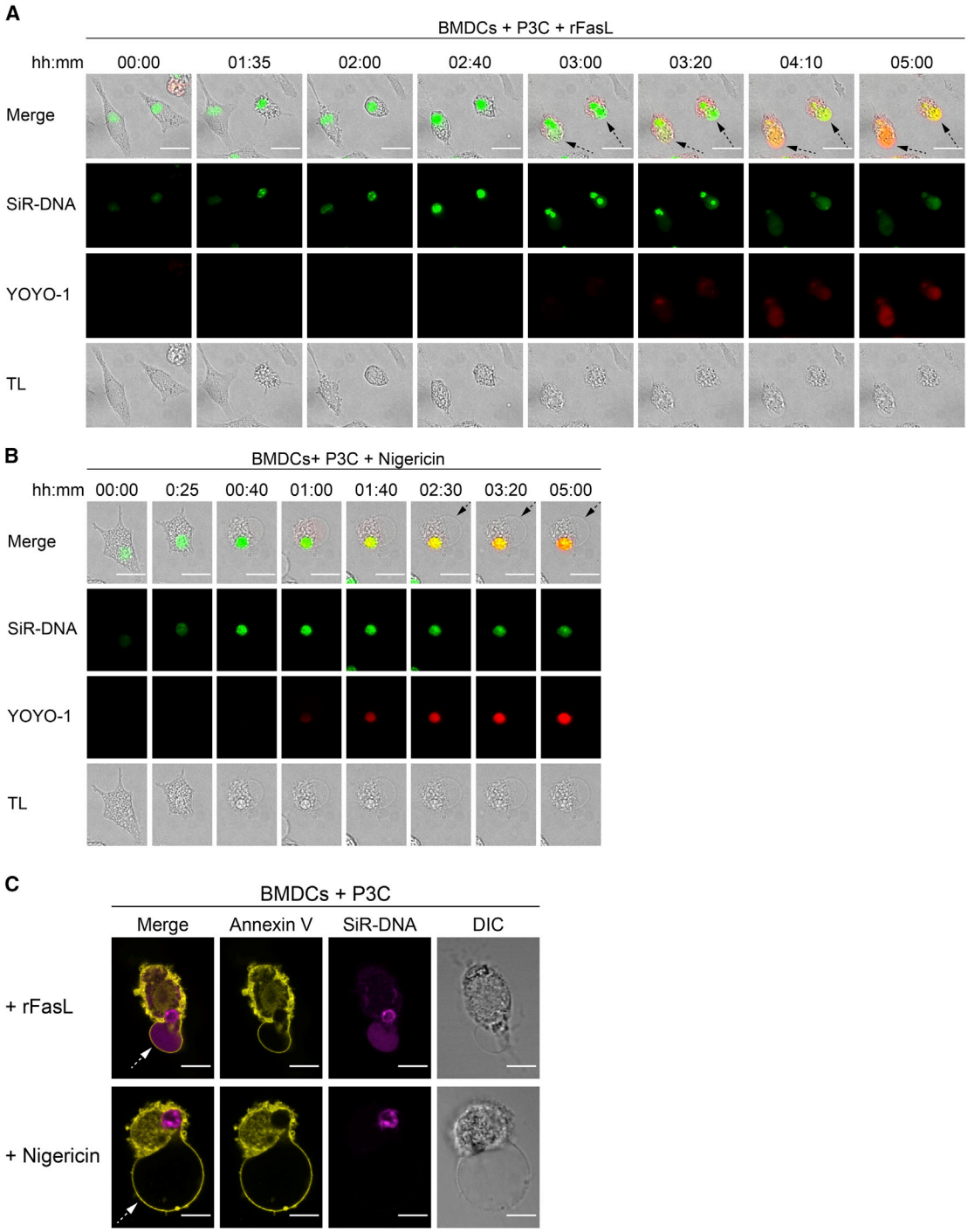

Figure 6. Nuclear DNA Diffuses to the Cytosol and Plasma Membrane Balloons in BMDCs When Necrosis Is Preceded by Apoptosis

(A and B) P3C-primed BMDCs were labeled with SiR-DNA and stimulated with rFasL (A) or nigericin (B). Morphological changes (TL), nuclear DNA (SiR-DNA, green), and YOYO-1 (red) staining were monitored by live imaging over 6 h. Images were captured every 5 min, and representative time points are shown. Dotted arrows point at necrotic plasma membrane balloons. The scale bars represent 10 μm.

(C) P3C-primed BMDCs were labeled with SiR-DNA and stimulated with (top) rFasL or (bottom) nigericin in the presence of annexin V. Morphological changes (TL), nuclear DNA (SiR-DNA, magenta), and annexin V (yellow) staining were assessed after 6 h of stimulation. Dotted arrows point at necrotic plasma membrane balloons. The scale bars represent 10 μm.

Panels are representative of at least three different experiments. See also Figure S5.

Fas Ligation Drives Pyroptosis and IL-1β Release by TLR-Primed BMDCs through the Pore-Forming Protein GSDMD

Following assembly of the Nlrp3 inflammasome, active caspase-1 not only processes pro-IL-1β but also cleaves the pore-forming protein GSDMD. The cleaved N-terminal domain of GSDMD interacts with the plasma membrane and oligomerizes, forming pores that serve as conduits for the release of IL-1β (Evavold et al., 2018; Heilig et al., 2018) and ultimately cause the cell to swell and lyse (Hagar et al., 2013; Liu et al., 2016; Shi et al., 2015). Given that FasL-induced IL-1β release by TLR-primed BMDCs was partially dependent on the Nlrp3 inflammasome (Figures 3A–3D), we next tested whether GSDMD contributed to IL-1β release and the progression to pyroptosis observed following Fas ligation. Consistent with published data, we found that nigericin-induced IL-1β release and pyroptosis were completely dependent on GSDMD. In contrast, the ability of GSDMD-deficient BMDCs to release IL-1β (Figure 7A) and become pyroptotic (Figure 7B) following Fas ligation was lost early on but was progressively regained over time. Analysis of GSDMD cleavage by immunoblot confirmed that Fas ligation resulted in processing of GSDMD into the pore-forming N-terminal fragment (Figure 7C). Fas ligation also resulted in generation of a GSDMD fragment of about 20 kDa (GSDMD inactive). The appearance of this 20-kDa band is consistent with previous reports showing that caspase-3 and -7 can inactivate GSDMD by cleaving it at aspartate 87 (Taabazuing et al., 2017), suggesting that this fragment may be the result of combined cleavage between caspase-1 and caspase-3 or -7. The abundance of this inactive fragment may partly explain the limited role of the Nlrp3 inflammasome and GSDMD in the late phase of FasL-induced pyroptosis and IL-1β release by TLR-primed BMDCs.

Given that loss of GSDMD appeared to have a more profound effect on IL-1β release and cell death than loss of the inflammasome components Nlrp3, caspase-1/11, or ASC (Figures 7A, 7B, and 3A–3D), we asked whether an alternative, inflammasome-independent pathway may be contributing to GSDMD cleavage following Fas ligation. Nlrp3 and caspase-1/11-deficient BMDCs were indeed still capable of cleaving GSDMD into its pore-forming fragment, albeit to a lesser extent than WT BMDCs (Figure S6A). Because caspase-8 has recently been shown to cleave GSDMD in the context of *Yersinia* infection (Orning et al., 2018; Sarhan et al., 2018), we asked whether caspase-8 was responsible for the inflammasome-independent processing of GSDMD downstream of Fas ligation. Although caspase-8-deficient BMDCs were unaffected in their ability to cleave GSDMD following nigericin-induced Nlrp3 inflammasome activation, they were completely unable to process GSDMD in response to Fas ligation (Figure S6B).

Following our observation that caspase-8 can induce GSDMD cleavage independent of the inflammasome, we hypothesized that GSDMD pores might mediate activation of the Nlrp3 inflammasome downstream of Fas ligation. Indeed, caspase-1 cleavage was significantly impaired in GSDMD-deficient BMDCs following Fas ligation (Figure 7D). Together, our data demonstrate that caspase-8 is the main driver of IL-1β release downstream of Fas ligation and that it does so by directly cleaving IL-1β and GSDMD. The resulting GSDMD-mediated pore formation likely leads to potassium efflux, activating the Nlrp3 inflammasome and amplifying IL-1β release.

In addition to GSDMD, pyroptosis has been reported to occur in response to chemotherapy drugs via caspase-3-mediated cleavage of gasdermin E (GSDME), another gasdermin family member with pore-forming activity (Wang et al., 2017). Moreover, the N-terminal fragment of GSDME has been shown to mediate breakdown of the plasma membrane during the late stages of apoptosis, driving the transition from apoptosis to secondary necrosis (Rogers et al., 2017). Because Fas ligation resulted in robust activation of caspase-3 (Figure 3E), we next asked whether GSDME was involved in FasL-induced IL-1β release and pyroptosis. Although GSDME was rapidly processed into its pore-forming N-terminal fragment (Figure 7C), the ability of GSDME-deficient BMDCs to process and secrete IL-1β (Figures 7E and 7G) or release LDH (Figure 7F) in response to Fas ligation remained intact. Further, analysis of caspase-1 and GSDMD cleavage revealed that GSDME did not play a role in FasL-induced inflammasome activation (Figure 7G). We also considered the possibility that a role of GSDME was obscured by the effect of GSDMD. To address this, we assessed IL-1β release in GSDMD$^{-/-}$GSMDE$^{-/-}$ double-knockout BMDCs but found no additional defect other than that observed in GSDMD single-deficient BMDCs (Figure 7H). These results suggest that the pore-forming activity of GSDMD, but not GSDME, drives IL-1β release and the transition from apoptosis to pyroptosis in TLR-primed BMDCs following Fas ligation.

We next sought to determine whether a two-cell model for IL-1β release could also be operative in humans. Human iNKT cells have been reported previously to induce IL-1β secretion by peripheral blood monocytes (Felley et al., 2016), although the mechanism through which they do this was not elucidated. We cultured P3C-primed human MDMs with iNKT cells in the presence of αGalCer. As in the mouse system, a priming signal was insufficient to elicit release of IL-1β by BMDCs, but addition of iNKT cells triggered IL-1β secretion to an extent comparable with that induced by nigericin (Figure S6C). Addition of rFasL to P3C-primed MDMs also resulted in significant release of IL-1β, and this effect was blocked by a FasL-neutralizing antibody (Figure S6D). Although rFasL was able to drive IL-1β release, we failed to observe inhibition of IL-1β release when two distinct FasL-blocking antibodies were individually added to the MDM-iNKT cell co-culture (data not shown). Thus, it appears that, although human MDMs can be triggered to secrete IL-1β by FasL (Figure S6D) and are also responsive to iNKT cells in co-culture (Figure S6C), human iNKT cells may employ additional molecules that can drive this pathway.

DISCUSSION

During infection, processing and secretion of IL-1β have mainly been thought to hinge on inflammasome activation following recognition of microbes in the host cell cytosol. However, pathogenic microorganisms employ a number of strategies to suppress or evade this cell-autonomous mechanism of inflammasome activation. Further, there are several examples of infections in which IL-1β plays an important protective role

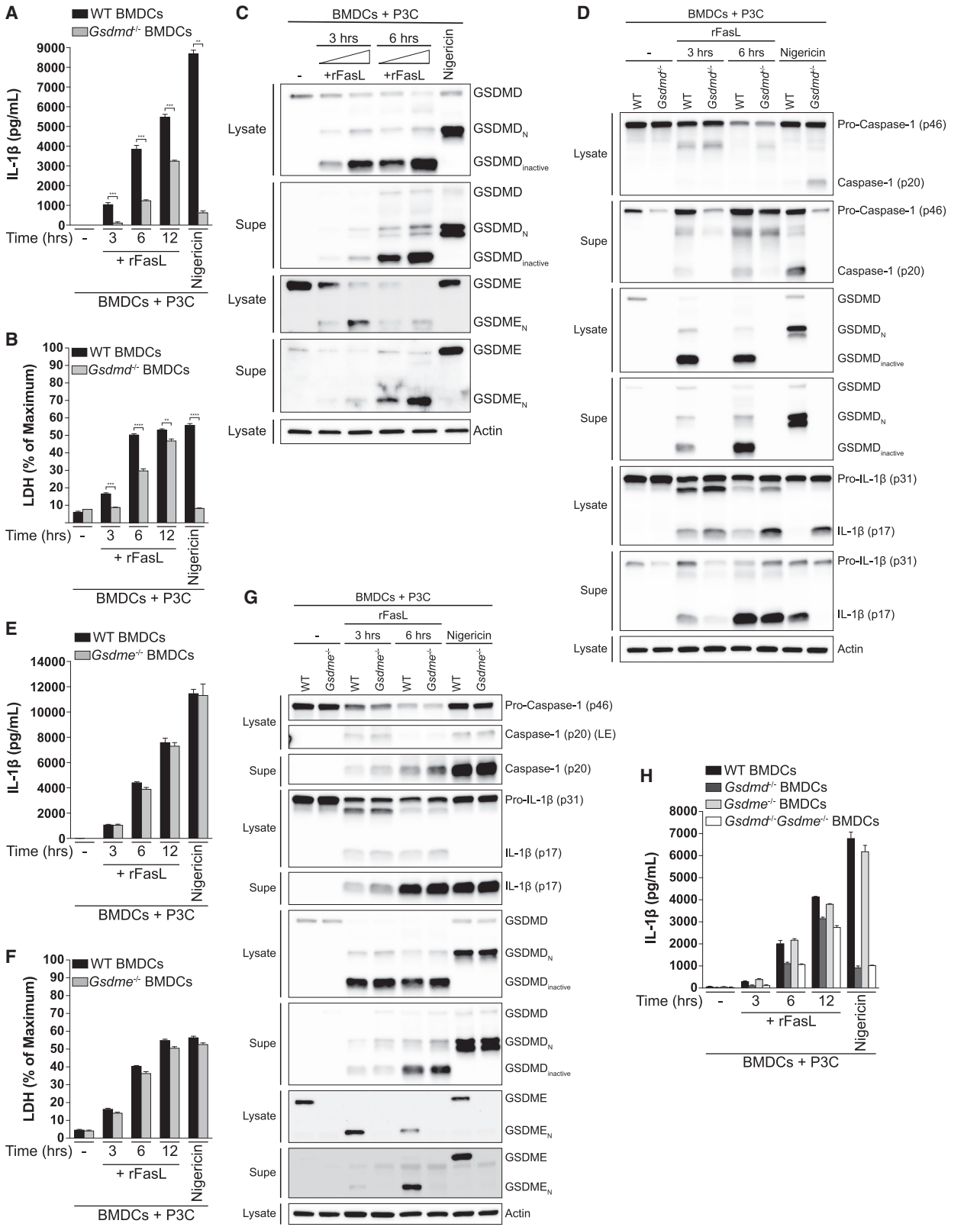

(legend on next page)

independent of caspase-1 or the inflammasomes, including infection with *C. trachomatis* (Bellocchio et al., 2004; Chen et al., 2016; Lu et al., 2000), *Pseudomonas aeruginosa* (Karmakar et al., 2012), and *Mycobacterium tuberculosis* (Dorhoi et al., 2012; Juffermans et al., 2000; McElvania Tekippe et al., 2010). These observations suggest that there are important mechanisms of IL-1β release in addition to the inflammasomes. The ability of iNKT cells to instruct BMDCs to process and secrete IL-1β represents an important mechanism by which the immune system could overcome microbial inflammasome evasion. Although cell-intrinsic cytosolic sensing by inflammasomes is undoubtedly important, perhaps it is not surprising that additional pathways to promote IL-1β release have evolved in the complex multicellular immune systems of mammals.

iNKT cells, "cellular adjuvants" of the immune system, are characterized by a number of features that endow them with the ability to respond to infection in an innate-like manner. They reside in a poised effector state and can respond within minutes to hours of being activated. Their ability to rapidly exert their effector functions is partly due to their constitutive expression of preformed cytokine-encoding mRNAs, a feature that does not require prior recognition of foreign antigen (Bendelac et al., 2007; Brennan et al., 2013; Cohen et al., 2013; Gutierrez-Arcelus et al., 2019; Kohlgruber et al., 2016; Liu et al., 2016). Our studies revealed that iNKT cells express FasL transcripts and protein at steady state and that they rapidly translocate pre-existing intracellular FasL stores to their surface following cognate interactions with TLR-primed BMDCs. These pre-existing FasL stores and the ability to rapidly deploy FasL to elicit IL-1β release by TLR-primed BMDCs are further evidence of the innate-like functional role of iNKT cells that distinguishes them from adaptive, MHC-restricted T cells.

iNKT cells recognize distinct endogenous and exogenous lipid antigens through a hotspot of invariant, germline-encoded residues in their TCR, a property that allows iNKT cells to respond *en masse*, essentially as a clonal population (Scott-Browne et al., 2007). This mode of recognition is very similar to how pattern recognition receptors (PRRs) recognize pathogen-associated molecular patterns (PAMPs) (Chuenchor et al., 2014). Based on our findings, we propose that the iNKT cell TCR can function as a surrogate PRR that may complement sensing of microbes that fail to elicit strong inflammasome activation from within the cytosol of an APC. We hypothesize that this alternative, two-cell mechanism of IL-1β release may permit specific recognition of microorganisms that have high pathogenic potential but fail to activate inflammasomes in a cell-autonomous manner. It is also conceivable that iNKT cells may trigger release of IL-1β by APCs that have been exposed to commensal microbes that otherwise do not activate the inflammasomes. This may occur in the liver, which captures gut commensal bacteria that enter the bloodstream during intestinal pathology (Balmer et al., 2014) and where iNKT cells make up to 30% of the lymphocyte compartment (Brennan et al., 2013). Both of these theories are supported by our findings that iNKT cells can elicit IL-1β release by BMDCs exposed to the obligate intracellular pathogen *C. trachomatis* (Figure 4B) or the gut commensal *B. fragilis* (Figure 4A). Because iNKT cells can be activated by bacteria, viruses, fungi, and even sterile inflammation, the mechanisms defined in this report provide a pathway for IL-1β release across a range of inflammatory situations.

Although iNKT cells can be activated through direct recognition of microbial lipids presented on CD1d, it is now appreciated that they may be even more frequently activated by mammalian self-lipid antigens induced in host cells by TLR agonists or infections, including microbes that do not harbor cognate lipid antigens (Brennan et al., 2011; Brigl et al., 2011; Salio et al., 2007). This provides a nearly universal mechanism of iNKT cell activation by mammalian cells that allows them to respond to a vast array of microorganisms with the simple requirement that a microbe engages a TLR on the APC. Importantly, here we found that iNKT cells can instruct TLR-primed BMDCs to secrete IL-1β in response to endogenous or foreign lipid antigens presented on CD1d. Thus, our studies suggest that any microorganism that stimulates a TLR on an APC could elicit activation of this two-cell pathway for IL-1β release.

We observed that iNKT cell-driven IL-1β release is mediated entirely through ligation of Fas on APCs. Fas ligation has been reported previously to drive secretion of IL-1β through caspase-8 independent of the Nlrp3 inflammasome (Bossaller et al., 2012; Miwa et al., 1998; Uchiyama et al., 2013). In contrast to these studies, we found that, although caspase-8 directly cleaves the majority of IL-1β secreted in response to Fas ligation (Figures 3B and 3F), it also cleaves GSDMD (Figures S6A and S6B) to induce Nlrp3 inflammasome activation. GSDMD-mediated pore formation then leads to potassium efflux, resulting in activation of the Nlrp3 inflammasome (Figures 3G and 3H) as a mechanism to amplify IL-1β release.

Apoptosis has long been regarded as an immunologically silent form of cell death. Classically, this feature is achieved through organized dismantling of the cell into apoptotic bodies

Figure 7. Fas Ligation Drives Pyroptosis and IL-1β Release by TLR-Primed BMDCs through the Pore-Forming Proteins GSDMD and GSDME

(A and B) P3C-primed BMDCs from WT and *Gsdmd*$^{-/-}$ mice were stimulated with rFasL for the indicated times. IL-1β release was quantified by ELISA (A), and LDH in the extracellular medium (B) was monitored by an enzymatic assay. Nigericin-treated BMDCs were used as a control.

(C and D) P3C-primed BMDCs from WT (C) or WT and *Gsdmd*$^{-/-}$ (D) mice were stimulated with rFasL for the indicated times, and the cell lysates and cell-free Supes were probed for the indicated proteins by immunoblot.

(E–G) P3C-primed BMDCs from WT and *Gsdme*$^{-/-}$ mice were treated with rFasL for the indicated times. IL-1β release was quantified by ELISA (E), LDH in the extracellular medium was monitored by an enzymatic assay (F), and the cell lysates and cell-free Supes were probed for the indicated proteins by immunoblot (G).

(H) P3C-primed BMDCs from WT, *Gsdmd*$^{-/-}$, *Gsdme*$^{-/-}$, and *Gsdmd*$^{-/-}$*Gsdme*$^{-/-}$ mice were stimulated with rFasL for the indicated times. IL-1β release was quantified by ELISA.

Error bars represent mean + SD. Each panel is representative of at least three different experiments. $^{**}p < 0.01$, $^{***}p < 0.001$, $^{****}p < 0.0001$, as determined by Student's unpaired t test. See also Figure S6.

that are rapidly taken up and cleared by phagocytes. As this process unfolds, the paradigm has remained that the plasma membrane preserves its integrity, preventing putative damage-associated molecular patterns (DAMPs) from leaking into the extracellular space and causing inflammation (Galluzzi et al., 2018). Nonetheless, several studies have shown that apoptosis is not always silent and can induce potent inflammatory responses *in vitro* and *in vivo* (Bossaller et al., 2012; Faouzi et al., 2001; Feltham et al., 2017). Secondary necrosis has been thought to occur when cells undergo the complete apoptotic program but are not scavenged by phagocytes. In contrast, we found that TLR-primed BMDCs initiate apoptosis, exhibiting cytoplasmic shrinkage and membrane blebbing that very rapidly progressed to cell swelling and lysis. Further, annexin V staining revealed that BMDCs did not always externalize phosphatidylserine prior to undergoing swelling, as would be expected during classical apoptosis, whereas cells that exposed phosphatidylserine did so for merely minutes before lysing. This suggests that TLR-primed BMDCs initiate the apoptotic program in response to Fas ligation but then rapidly switch to pyroptosis through the action of the pore-forming protein GSDMD. Of note, although we found that GSDMD plays a major role in FasL-induced IL-1β release and cell death, GSDMD-deficient BMDCs were still capable of releasing IL-1β and undergoing necrosis at late time points (Figures 7A and 7B). Given our observation that GSDME does not play a role in FasL-induced IL-1β or cell death (Figures 7E and 7F), it is conceivable that other pore-forming proteins are activated late during execution of apoptosis and that these can compensate for the lack of GSDMD. Taken together, our findings demonstrate that iNKT cells can co-opt the extrinsic apoptotic pathway to instruct TLR-primed BMDCs to undergo an inflammatory form of cell death characterized by release of bioactive IL-1β, a fascinating repurposing of signaling modules that evolved for cell death and cytoplasmic danger sensing.

In summary, we described a two-cell model for IL-1β release where iNKT cells employ FasL to instruct TLR-primed BMDCs to process and secrete IL-1β. This is made possible by the ability of iNKT cells to rapidly translocate pre-existing intracellular FasL stores to their surface following cognate interactions. Therefore, iNKT cells are positioned to rapidly instruct APCs to secrete IL-1β, and they can do so following infection with any microorganism that stimulates a PRR on APCs (Figure S7). This mechanism may also be at play in the setting of non-infectious or sterile inflammation, where FasL-expressing T cells may drive the autoimmune pathology associated with dysregulated IL-1β release. We show that, in addition to "ancient" cell-autonomous cytosolic sensing by inflammasomes, mammals have evolved a multi-cellular, cell-extrinsic pathway for IL-1β release that combines signaling components of the inflammasomes and the extrinsic cell death pathways. Our study provides a mandate to examine the likely possibility that other innate-like T cells, including γδ T cells, mucosa-associated invariant T cells, and even adaptive effector T cells, can also co-opt the death receptor pathway to provide the innate immune system with cell-extrinsic IL-1β secretion signals.

STAR★METHODS

Detailed methods are provided in the online version of this paper and include the following:

- KEY RESOURCES TABLE
- LEAD CONTACT AND MATERIALS AVAILABILITY
- EXPERIMENTAL MODEL AND SUBJECT DETAILS
  - Mice
  - Bacterial strains and growth
  - Human samples
- METHOD DETAILS
  - Preparation of murine bone marrow-derived dendritic cells (BMDCs)
  - Preparation of human monocyte-derived macrophages (MDMs)
  - Generation of iNKT cell lines
  - Cell stimulation
  - ELISAs and LDH release assays
  - Flow Cytometric Analysis of FasL Expression
  - Immunoblotting
  - Flow Cytometric Quantification of Cell Death
  - Live Imaging of Cell Death
  - TUNEL staining
  - Cell Sorting
  - Bacterial Infections
  - ImmGen expression data
- QUANTIFICATION AND STATISTICAL ANALYSIS
- DATA AND CODE AVAILABILITY

SUPPLEMENTAL INFORMATION

Supplemental Information can be found online at https://doi.org/10.1016/j.celrep.2020.03.030.

ACKNOWLEDGMENTS

We thank Warren Alexander (*Mlkl*$^{-/-}$), Hongbo Luo (*Gsdmd*$^{-/-}$), Edward Mocarski (*Ripk3*$^{-/-}$ and *Ripk3*$^{-/-}$*Casp8*$^{-/-}$), Petr Broz (*Gsdme*$^{-/-}$ and *Gsdmd*$^{-/-}$*Gsdme*$^{-/-}$), Igor Brodsky (*Caspase-8*$^{DA/DA}$), and Gabriel Nuñez (*Asc*$^{-/-}$) for providing bone marrow from valuable mice. We thank Michael Starnbach and Eric Dumas for providing *C. trachomatis* serovar D (UW-3/Cx; ATCC) and Laurie Comstock for providing *B. fragilis* (NCTC 9343). This work was supported by NIH grants R21 AI44139, R01 AI44139, and R01 AI063428 (to M.B.B.); K08 AI102945 (to P.J.B.); institutional training grants T32 HL007627 and K08 AR075850 (to D.P.S.); and R01 HL124209 and funding from the American Asthma Foundation, Alex's Lemonade Stand Foundation for Childhood Cancer, and the V Foundation for Cancer Research (to B.A.C.). We thank Jonathan C. Kagan for helpful discussions. The following reagent was obtained through the NIH Tetramer Core Facility: APC-conjugated CD1d tetramer loaded with PBS-57 lipid antigen.

AUTHOR CONTRIBUTIONS

Conceptualization, C.A.D., P.J.B., and M.B.B.; Methodology, C.A.D.; Investigation, C.A.D., A.B.C., and D.P.S.; Resources, B.A.C.; Writing – Original Draft, C.A.D.; Writing – Review & Editing, C.A.D., P.J.B., M.B.B., and B.A.C.; Supervision, M.B.B. and P.J.B.; Funding Acquisition, M.B.B.

DECLARATION OF INTERESTS

The authors declare no competing interests.

Received: June 4, 2019
Revised: December 19, 2019
Accepted: March 10, 2020
Published: April 7, 2020

REFERENCES

Aglietti, R.A., Estevez, A., Gupta, A., Ramirez, M.G., Liu, P.S., Kayagaki, N., Ciferri, C., Dixit, V.M., and Dueber, E.C. (2016). GsdmD p30 elicited by caspase-11 during pyroptosis forms pores in membranes. Proc. Natl. Acad. Sci. USA *113*, 7858–7863.

Balmer, M.L., Slack, E., de Gottardi, A., Lawson, M.A., Hapfelmeier, S., Miele, L., Grieco, A., Van Vlierberghe, H., Fahrner, R., Patuto, N., et al. (2014). The liver may act as a firewall mediating mutualism between the host and its gut commensal microbiota. Sci. Transl. Med. *6*, 237ra66.

Bellocchio, S., Montagnoli, C., Bozza, S., Gaziano, R., Rossi, G., Mambula, S.S., Vecchi, A., Mantovani, A., Levitz, S.M., and Romani, L. (2004). The contribution of the Toll-like/IL-1 receptor superfamily to innate and adaptive immunity to fungal pathogens in vivo. J. Immunol. *172*, 3059–3069.

Bendelac, A., Savage, P.B., and Teyton, L. (2007). The biology of NKT cells. Annu. Rev. Immunol. *25*, 297–336.

Boatright, K.M., Deis, C., Denault, J.B., Sutherlin, D.P., and Salvesen, G.S. (2004). Activation of caspases-8 and -10 by FLIP(L). Biochem. J. *382*, 651–657.

Bossaller, L., Chiang, P.I., Schmidt-Lauber, C., Ganesan, S., Kaiser, W.J., Rathinam, V.A., Mocarski, E.S., Subramanian, D., Green, D.R., Silverman, N., et al. (2012). Cutting edge: FAS (CD95) mediates noncanonical IL-1β and IL-18 maturation via caspase-8 in an RIP3-independent manner. J. Immunol. *189*, 5508–5512.

Brennan, P.J., Tatituri, R.V., Brigl, M., Kim, E.Y., Tuli, A., Sanderson, J.P., Gadola, S.D., Hsu, F.F., Besra, G.S., and Brenner, M.B. (2011). Invariant natural killer T cells recognize lipid self antigen induced by microbial danger signals. Nat. Immunol. *12*, 1202–1211.

Brennan, P.J., Brigl, M., and Brenner, M.B. (2013). Invariant natural killer T cells: an innate activation scheme linked to diverse effector functions. Nat. Rev. Immunol. *13*, 101–117.

Brigl, M., van den Elzen, P., Chen, X., Meyers, J.H., Wu, D., Wong, C.-H., Reddington, F., Illarianov, P.A., Besra, G.S., Brenner, M.B., and Gumperz, J.E. (2006). Conserved and heterogeneous lipid antigen specificities of CD1d-restricted NKT cell receptors. J. Immunol. *176*, 3625–3634.

Brigl, M., Tatituri, R.V., Watts, G.F., Bhowruth, V., Leadbetter, E.A., Barton, N., Cohen, N.R., Hsu, F.F., Besra, G.S., and Brenner, M.B. (2011). Innate and cytokine-driven signals, rather than microbial antigens, dominate in natural killer T cell activation during microbial infection. J. Exp. Med. *208*, 1163–1177.

Broz, P., and Dixit, V.M. (2016). Inflammasomes: mechanism of assembly, regulation and signalling. Nat. Rev. Immunol. *16*, 407–420.

Chen, K., Shanmugam, N.K., Pazos, M.A., Hurley, B.P., and Cherayil, B.J. (2016). Commensal Bacteria-Induced Inflammasome Activation in Mouse and Human Macrophages Is Dependent on Potassium Efflux but Does Not Require Phagocytosis or Bacterial Viability. PLoS ONE *11*, e0160937.

Chen, K.W., Demarco, B., Heilig, R., Shkarina, K., Boettcher, A., Farady, C.J., Pelczar, P., and Broz, P. (2019). Extrinsic and intrinsic apoptosis activate pannexin-1 to drive NLRP3 inflammasome assembly. EMBO J. *38*.

Chiba, A., Cohen, N., Brigl, M., Brennan, P.J., Besra, G.S., and Brenner, M.B. (2009). Rapid and reliable generation of invariant natural killer T-cell lines in vitro. Immunology *128*, 324–333.

Chuenchor, W., Jin, T., Ravilious, G., and Xiao, T.S. (2014). Structures of pattern recognition receptors reveal molecular mechanisms of autoinhibition, ligand recognition and oligomerization. Curr. Opin. Immunol. *26*, 14–20.

Cohen, N.R., Brennan, P.J., Shay, T., Watts, G.F., Brigl, M., Kang, J., and Brenner, M.B.; ImmGen Project Consortium (2013). Shared and distinct transcriptional programs underlie the hybrid nature of iNKT cells. Nat. Immunol. *14*, 90–99.

Dinarello, C.A. (2011). A clinical perspective of IL-1β as the gatekeeper of inflammation. Eur. J. Immunol. *41*, 1203–1217.

Ding, J., Wang, K., Liu, W., She, Y., Sun, Q., Shi, J., Sun, H., Wang, D.C., and Shao, F. (2016). Pore-forming activity and structural autoinhibition of the gasdermin family. Nature *535*, 111–116.

Dorhoi, A., Nouailles, G., Jörg, S., Hagens, K., Heinemann, E., Pradl, L., Oberbeck-Müller, D., Duque-Correa, M.A., Reece, S.T., Ruland, J., et al. (2012). Activation of the NLRP3 inflammasome by Mycobacterium tuberculosis is uncoupled from susceptibility to active tuberculosis. Eur. J. Immunol. *42*, 374–384.

Erlich, Z., Shlomovitz, I., Edry-Botzer, L., Cohen, H., Frank, D., Wang, H., Lew, A.M., Lawlor, K.E., Zhan, Y., Vince, J.E., and Gerlic, M. (2019). Macrophages, rather than DCs, are responsible for inflammasome activity in the GM-CSF BMDC model. Nat. Immunol. *20*, 397–406.

Evavold, C.L., Ruan, J., Tan, Y., Xia, S., Wu, H., and Kagan, J.C. (2018). The Pore-Forming Protein Gasdermin D Regulates Interleukin-1 Secretion from Living Macrophages. Immunity *48*, 35–44.e6.

Exley, M.A., Bigley, N.J., Cheng, O., Shaulov, A., Tahir, S.M., Carter, Q.L., Garcia, J., Wang, C., Patten, K., Stills, H.F., et al. (2003). Innate immune response to encephalomyocarditis virus infection mediated by CD1d. Immunology *110*, 519–526.

Faouzi, S., Burckhardt, B.E., Hanson, J.C., Campe, C.B., Schrum, L.W., Rippe, R.A., and Maher, J.J. (2001). Anti-Fas induces hepatic chemokines and promotes inflammation by an NF-kappa B-independent, caspase-3-dependent pathway. J. Biol. Chem. *276*, 49077–49082.

Felley, L.E., Sharma, A., Theisen, E., Romero-Masters, J.C., Sauer, J.D., and Gumperz, J.E. (2016). Human Invariant NKT Cells Induce IL-1β Secretion by Peripheral Blood Monocytes via a P2X7-Independent Pathway. J. Immunol. *197*, 2455–2464.

Feltham, R., Vince, J.E., and Lawlor, K.E. (2017). Caspase-8: not so silently deadly. Clin. Transl. Immunology *6*, e124.

Galluzzi, L., Kepp, O., Chan, F.K., and Kroemer, G. (2017). Necroptosis: Mechanisms and Relevance to Disease. Annu. Rev. Pathol. *12*, 103–130.

Galluzzi, L., Vitale, I., Aaronson, S.A., Abrams, J.M., Adam, D., Agostinis, P., Alnemri, E.S., Altucci, L., Amelio, I., Andrews, D.W., et al. (2018). Molecular mechanisms of cell death: recommendations of the Nomenclature Committee on Cell Death 2018. Cell Death Differ. *25*, 486–541.

Green, D.R., and Llambi, F. (2015). Cell Death Signaling. Cold Spring Harb. Perspect. Biol. *7*.

Gutierrez-Arcelus, M., Teslovich, N., Mola, A.R., Polidoro, R.B., Nathan, A., Kim, H., Hannes, S., Slowikowski, K., Watts, G.F.M., Korsunsky, I., et al. (2019). Lymphocyte innateness defined by transcriptional states reflects a balance between proliferation and effector functions. Nat. Commun. *10*, 687.

Hagar, J.A., Powell, D.A., Aachoui, Y., Ernst, R.K., and Miao, E.A. (2013). Cytoplasmic LPS activates caspase-11: implications in TLR4-independent endotoxic shock. Science *341*, 1250–1253.

Heilig, R., Dick, M.S., Sborgi, L., Meunier, E., Hiller, S., and Broz, P. (2018). The Gasdermin-D pore acts as a conduit for IL-1β secretion in mice. Eur. J. Immunol. *48*, 584–592.

Helft, J., Böttcher, J., Chakravarty, P., Zelenay, S., Huotari, J., Schraml, B.U., Goubau, D., and Reis e Sousa, C. (2015). GM-CSF Mouse Bone Marrow Cultures Comprise a Heterogeneous Population of CD11c(+)MHCII(+) Macrophages and Dendritic Cells. Immunity *42*, 1197–1211.

Heng, T.S., and Painter, M.W.; Immunological Genome Project Consortium (2008). The Immunological Genome Project: networks of gene expression in immune cells. Nat. Immunol. *9*, 1091–1094.

Higa, N., Toma, C., Nohara, T., Nakasone, N., Takaesu, G., and Suzuki, T. (2013). Lose the battle to win the war: bacterial strategies for evading host inflammasome activation. Trends Microbiol. *21*, 342–349.

Holler, N., Tardivel, A., Kovacsovics-Bankowski, M., Hertig, S., Gaide, O., Martinon, F., Tinel, A., Deperthes, D., Calderara, S., Schulthess, T., et al. (2003). Two adjacent trimeric Fas ligands are required for Fas signaling and formation of a death-inducing signaling complex. Mol. Cell. Biol. *23*, 1428–1440.

Juffermans, N.P., Florquin, S., Camoglio, L., Verbon, A., Kolk, A.H., Speelman, P., van Deventer, S.J., and van Der Poll, T. (2000). Interleukin-1 signaling is essential for host defense during murine pulmonary tuberculosis. J. Infect. Dis. *182*, 902–908.

Kaiser, W.J., Upton, J.W., Long, A.B., Livingston-Rosanoff, D., Daley-Bauer, L.P., Hakem, R., Caspary, T., and Mocarski, E.S. (2011). RIP3 mediates the embryonic lethality of caspase-8-deficient mice. Nature *471*, 368–372.

Kambara, H., Liu, F., Zhang, X., Liu, P., Bajrami, B., Teng, Y., Zhao, L., Zhou, S., Yu, H., Zhou, W., et al. (2018). Gasdermin D Exerts Anti-inflammatory Effects by Promoting Neutrophil Death. Cell Rep. *22*, 2924–2936.

Karmakar, M., Sun, Y., Hise, A.G., Rietsch, A., and Pearlman, E. (2012). Cutting edge: IL-1β processing during Pseudomonas aeruginosa infection is mediated by neutrophil serine proteases and is independent of NLRC4 and caspase-1. J. Immunol. *189*, 4231–4235.

Kayagaki, N., Stowe, I.B., Lee, B.L., O'Rourke, K., Anderson, K., Warming, S., Cuellar, T., Haley, B., Roose-Girma, M., Phung, Q.T., et al. (2015). Caspase-11 cleaves gasdermin D for non-canonical inflammasome signalling. Nature *526*, 666–671.

Kim, E.Y., Lynch, L., Brennan, P.J., Cohen, N.R., and Brenner, M.B. (2015). The transcriptional programs of iNKT cells. Semin. Immunol. *27*, 26–32.

Kohlgruber, A.C., Donado, C.A., LaMarche, N.M., Brenner, M.B., and Brennan, P.J. (2016). Activation strategies for invariant natural killer T cells. Immunogenetics *68*, 649–663.

Kovacs, S.B., and Miao, E.A. (2017). Gasdermins: Effectors of Pyroptosis. Trends Cell Biol. *27*, 673–684.

Kovarova, M., Hesker, P.R., Jania, L., Nguyen, M., Snouwaert, J.N., Xiang, Z., Lommatzsch, S.E., Huang, M.T., Ting, J.P., and Koller, B.H. (2012). NLRP1-dependent pyroptosis leads to acute lung injury and morbidity in mice. J. Immunol. *189*, 2006–2016.

Kuida, K., Lippke, J.A., Ku, G., Harding, M.W., Livingston, D.J., Su, M.S., and Flavell, R.A. (1995). Altered cytokine export and apoptosis in mice deficient in interleukin-1 beta converting enzyme. Science *267*, 2000–2003.

Latz, E., Xiao, T.S., and Stutz, A. (2013). Activation and regulation of the inflammasomes. Nat. Rev. Immunol. *13*, 397–411.

Liu, X., Zhang, Z., Ruan, J., Pan, Y., Magupalli, V.G., Wu, H., and Lieberman, J. (2016). Inflammasome-activated gasdermin D causes pyroptosis by forming membrane pores. Nature *535*, 153–158.

Lu, H., Shen, C., and Brunham, R.C. (2000). Chlamydia trachomatis infection of epithelial cells induces the activation of caspase-1 and release of mature IL-18. J. Immunol. *165*, 1463–1469.

Maltez, V.I., and Miao, E.A. (2016). Reassessing the Evolutionary Importance of Inflammasomes. J. Immunol. *196*, 956–962.

Martinon, F., Burns, K., and Tschopp, J. (2002). The inflammasome: a molecular platform triggering activation of inflammatory caspases and processing of proIL-beta. Mol. Cell *10*, 417–426.

McElvania Tekippe, E., Allen, I.C., Hulseberg, P.D., Sullivan, J.T., McCann, J.R., Sandor, M., Braunstein, M., and Ting, J.P. (2010). Granuloma formation and host defense in chronic Mycobacterium tuberculosis infection requires PYCARD/ASC but not NLRP3 or caspase-1. PLoS ONE *5*, e12320.

Miao, E.A., Rajan, J.V., and Aderem, A. (2011). Caspase-1-induced pyroptotic cell death. Immunol. Rev. *243*, 206–214.

Micheau, O., Thome, M., Schneider, P., Holler, N., Tschopp, J., Nicholson, D.W., Briand, C., and Grütter, M.G. (2002). The long form of FLIP is an activator of caspase-8 at the Fas death-inducing signaling complex. J. Biol. Chem. *277*, 45162–45171.

Miwa, K., Asano, M., Horai, R., Iwakura, Y., Nagata, S., and Suda, T. (1998). Caspase 1-independent IL-1beta release and inflammation induced by the apoptosis inducer Fas ligand. Nat. Med. *4*, 1287–1292.

Muñoz-Planillo, R., Kuffa, P., Martínez-Colón, G., Smith, B.L., Rajendiran, T.M., and Núñez, G. (2013). K^+ efflux is the common trigger of NLRP3 inflammasome activation by bacterial toxins and particulate matter. Immunity *38*, 1142–1153.

Murphy, J.M., Czabotar, P.E., Hildebrand, J.M., Lucet, I.S., Zhang, J.G., Alvarez-Diaz, S., Lewis, R., Lalaoui, N., Metcalf, D., Webb, A.I., et al. (2013). The pseudokinase MLKL mediates necroptosis via a molecular switch mechanism. Immunity *39*, 443–453.

Nagata, S. (2018). Apoptosis and Clearance of Apoptotic Cells. Annu. Rev. Immunol. *36*, 489–517.

Newton, K., Sun, X., and Dixit, V.M. (2004). Kinase RIP3 is dispensable for normal NF-kappa Bs, signaling by the B-cell and T-cell receptors, tumor necrosis factor receptor 1, and Toll-like receptors 2 and 4. Mol. Cell. Biol. *24*, 1464–1469.

Oberst, A., Dillon, C.P., Weinlich, R., McCormick, L.L., Fitzgerald, P., Pop, C., Hakem, R., Salvesen, G.S., and Green, D.R. (2011). Catalytic activity of the caspase-8-FLIP(L) complex inhibits RIPK3-dependent necrosis. Nature *471*, 363–367.

Orning, P., Weng, D., Starheim, K., Ratner, D., Best, Z., Lee, B., Brooks, A., Xia, S., Wu, H., Kelliher, M.A., et al. (2018). Pathogen blockade of TAK1 triggers caspase-8-dependent cleavage of gasdermin D and cell death. Science *362*, 1064–1069.

Ozören, N., Masumoto, J., Franchi, L., Kanneganti, T.-D., Body-Malapel, M., Ertürk, I., Jagirdar, R., Zhu, L., Inohara, N., Bertin, J., et al. (2006). Distinct roles of TLR2 and the adaptor ASC in IL-1β/IL-18 secretion in response to Listeria monocytogenes. J. Immunol. *176*, 4337–4342.

Philip, N.H., DeLaney, A., Peterson, L.W., Santos-Marrero, M., Grier, J.T., Sun, Y., Wynosky-Dolfi, M.A., Zwack, E.E., Hu, B., Olsen, T.M., et al. (2016). Activity of Uncleaved Caspase-8 Controls Anti-bacterial Immune Defense and TLR-Induced Cytokine Production Independent of Cell Death. PLoS Pathog. *12*, e1005910.

Pop, C., Oberst, A., Drag, M., Van Raam, B.J., Riedl, S.J., Green, D.R., and Salvesen, G.S. (2011). FLIP(L) induces caspase 8 activity in the absence of interdomain caspase 8 cleavage and alters substrate specificity. Biochem. J. *433*, 447–457.

Rogers, C., Fernandes-Alnemri, T., Mayes, L., Alnemri, D., Cingolani, G., and Alnemri, E.S. (2017). Cleavage of DFNA5 by caspase-3 during apoptosis mediates progression to secondary necrotic/pyroptotic cell death. Nat. Commun. *8*, 14128.

Salio, M., Speak, A.O., Shepherd, D., Polzella, P., Illarionov, P.A., Veerapen, N., Besra, G.S., Platt, F.M., and Cerundolo, V. (2007). Modulation of human natural killer T cell ligands on TLR-mediated antigen-presenting cell activation. Proc. Natl. Acad. Sci. USA *104*, 20490–20495.

Sarhan, J., Liu, B.C., Muendlein, H.I., Li, P., Nilson, R., Tang, A.Y., Rongvaux, A., Bunnell, S.C., Shao, F., Green, D.R., and Poltorak, A. (2018). Caspase-8 induces cleavage of gasdermin D to elicit pyroptosis during *Yersinia* infection. Proc. Natl. Acad. Sci. USA *115*, E10888–E10897.

Sborgi, L., Rühl, S., Mulvihill, E., Pipercevic, J., Heilig, R., Stahlberg, H., Farady, C.J., Müller, D.J., Broz, P., and Hiller, S. (2016). GSDMD membrane pore formation constitutes the mechanism of pyroptotic cell death. EMBO J. *35*, 1766–1778.

Schroder, K., and Tschopp, J. (2010). The inflammasomes. Cell *140*, 821–832.

Scott-Browne, J.P., Matsuda, J.L., Mallevaey, T., White, J., Borg, N.A., McCluskey, J., Rossjohn, J., Kappler, J., Marrack, P., and Gapin, L. (2007). Germline-encoded recognition of diverse glycolipids by natural killer T cells. Nat. Immunol. *8*, 1105–1113.

Shi, J., Zhao, Y., Wang, K., Shi, X., Wang, Y., Huang, H., Zhuang, Y., Cai, T., Wang, F., and Shao, F. (2015). Cleavage of GSDMD by inflammatory caspases determines pyroptotic cell death. Nature *526*, 660–665.

Shi, J., Gao, W., and Shao, F. (2017). Pyroptosis: Gasdermin-Mediated Programmed Necrotic Cell Death. Trends Biochem. Sci. *42*, 245–254.

Shin, S., and Brodsky, I.E. (2015). The inflammasome: Learning from bacterial evasion strategies. Semin. Immunol. *27*, 102–110.

Silke, J., Rickard, J.A., and Gerlic, M. (2015). The diverse role of RIP kinases in necroptosis and inflammation. Nat. Immunol. *16*, 689–697.

Stewart, M.K., and Cookson, B.T. (2016). Evasion and interference: intracellular pathogens modulate caspase-dependent inflammatory responses. Nat. Rev. Microbiol. *14*, 346–359.

Strasser, A., Jost, P.J., and Nagata, S. (2009). The many roles of FAS receptor signaling in the immune system. Immunity *30*, 180–192.

Swanson, K.V., Deng, M., and Ting, J.P. (2019). The NLRP3 inflammasome: molecular activation and regulation to therapeutics. Nat. Rev. Immunol. *19*, 477–489.

Taabazuing, C.Y., Okondo, M.C., and Bachovchin, D.A. (2017). Pyroptosis and Apoptosis Pathways Engage in Bidirectional Crosstalk in Monocytes and Macrophages. Cell Chem. Biol. *24*, 507–514.e4.

Tummers, B., and Green, D.R. (2017). Caspase-8: regulating life and death. Immunol. Rev. *277*, 76–89.

Uchiyama, R., Yonehara, S., and Tsutsui, H. (2013). Fas-mediated inflammatory response in Listeria monocytogenes infection. J. Immunol. *190*, 4245–4254.

Ulland, T.K., Ferguson, P.J., and Sutterwala, F.S. (2015). Evasion of inflammasome activation by microbial pathogens. J. Clin. Invest. *125*, 469–477.

Wang, Y., Gao, W., Shi, X., Ding, J., Liu, W., He, H., Wang, K., and Shao, F. (2017). Chemotherapy drugs induce pyroptosis through caspase-3 cleavage of a gasdermin. Nature *547*, 99–103.

STAR★METHODS

KEY RESOURCES TABLE

REAGENT or RESOURCE	SOURCE	IDENTIFIER
Antibodies		
Goat polyclonal anti-IL-1β	R&D Systems	Cat#AF-401-NA; RRID:AB_416684
Rabbit polyclonal anti-IL-1β	Genetex	Cat#GTX74034; RRID:AB_378141
Mouse monoclonal anti-Caspase-1 (clone Casper-1)	Adipogen	Cat#AG-20B-0042-C100; RRID:AB_2755041
Rat monoclonal anti-Caspase-8 (clone 1G12)	Enzo Life Sciences	Cat#ALX-804-447-C100; RRID:AB_2050952
Rabbit monoclonal anti-cleaved Caspase-8 (clone D5B2)	Cell Signaling Technology	Cat#8592; RRID:AB_10891784
Rabbit polyclonal anti-Caspase-3	Cell Signaling Technology	Cat#9662; RRID:AB_331439
Rabbit polyclonal anti-cleaved Caspase-3	Cell Signaling Technology	Cat#9661; RRID:AB_2341188
Rabbit monoclonal anti-FLIP (clone D5J1E)	Cell Signaling Technology	Cat#56343; RRID:AB_2799508
Rabbit polyclonal anti-Caspase-6	Cell Signaling Technology	Cat#9762; RRID:AB_10829240
Rabbit monoclonal anti-Caspase-7 (clone D2Q3L)	Cell Signaling Technology	Cat#12827; RRID:AB_2687912
Mouse monoclonal anti-Caspase-9 (clone C9)	Cell Signaling Technology	Cat#9508; RRID:AB_2068620
Rabbit monoclonal anti-GSDMD (clone EPR19828)	Abcam	Cat#ab209845; RRID:AB_2783550
Rabbit monoclonal anti-DFNA5/GSDME (clone EPR19859)	Abcam	Cat#ab215191; RRID:AB_2737000
Mouse monoclonal anti-actin (clone AC-15)	Sigma-Aldrich	Cat#A5441; RRID:AB_476744
Anti-mouse CD11c (clone N418)	Thermo Fisher	Cat#MCD11c05; RRID:AB_10373550
Anti-mouse I-A/I-E (clone M5/114.15.2)	Thermo Fisher	Cat#46-5321-82; RRID:AB_1834439
Anti-mouse CD11b (clone M1/70)	Thermo Fisher	Cat#11-0112-82; RRID:AB_464935
Anti-mouse CD115 (clone AFS98)	Thermo Fisher	Cat#17-1152-82; RRID:AB_1210789
Anti-mouse CD135 (clone A2F10)	Thermo Fisher	Cat#12-1351-82; RRID:AB_465859
Anti-mouse MerTK (clone DS5MMER)	Thermo Fisher	Cat#25-5751-82; RRID:AB_2573466
Anti-mouse TCR β chain (clone H57-597)	Biolegend	Cat#109229; RRID:AB_10933263
Anti-mouse CD3 (clone 145-2C11)	Biolegend	Cat#100340; RRID:AB_11149115
Anti-mouse FasL (clone MFL3)	Biolegend	Cat#106606; RRID:AB_313279
Anti-phycoerythrin antibody (clone PE001)	Biolegend	Cat#408102; RRID:AB_2168924
Anti-mouse FasL blocking antibody (clone MFL3)	Biolegend	Cat#106612; RRID:AB_2813954
Armenian Hamster IgG isotype control antibody	Biolegend	Cat#400940; RRID:AB_11203529
Anti-human FasL blocking antibody (clone NOK-1)	Biolegend	Cat#306415; RRID:AB_2810458
Mouse IgG1, κ isotype control antibody (clone MOPC-21)	Biolegend	Cat#400165; RRID:AB_11150399
Biotinylated polyclonal goat anti-mouse IL-1β	R&D Systems	Cat#BAF401; RRID:AB_356450
Goat anti-mouse IgG (H+L)	Jackson ImmunoResearch	Cat#115-035-146; RRID:AB_2307392
Donkey anti-Rabbit IgG (H+L)	Jackson ImmunoResearch	Cat#711-035-152; RRID:AB_10015282
Donkey anti-Rat IgG (H+L)	Jackson ImmunoResearch	Cat#712-035-150; RRID:AB_2340638
Bovine anti-Goat IgG (H+L)	Jackson ImmunoResearch	Cat#805-035-180; RRID:AB_2340874
Rat anti-mouse CD16/CD32 (clone 93)	Thermo Fisher	Cat#16-0161-86; RRID:AB_468900
Bacterial and Virus Strains		
Bacteroidis fragilis (strain NCTC 9343)	Laboratory of Dr. Laurie Comstock	ATCC 25285
Chlamydia trachomatis (strain D/UW-3/Cx)	Laboratory of Dr. Michael Starnbach	ATCC VR-85
Biological Samples		
Human peripheral blood mononuclear cells	Brigham and Women's Hospital Kraft Family Blood Donor Center	N/A

(*Continued on next page*)

Continued

REAGENT or RESOURCE	SOURCE	IDENTIFIER
Chemicals, Peptides, and Recombinant Proteins		
Recombinant, multimeric FasL (MegaFasL)	Adipogen	Cat#AG-40B-0130-C010
Pam3CSK4	Invivogen	Cat#tlrl-pms
Nigericin	Invivogen	Cat#tlrl-nig
MSU Crystals	Invivogen	Cat#tlrl-msu
Alpha Galactosylceramide	Dr. Gurdyal Besra	N/A
Recombinant murine GM-CSF	Peprotech	Cat#315-03
Recombinant human GM-CSF	Peprotech	Cat#300-03
Recombinant murine IL-2	Peprotech	Cat#212-12
Recombinant murine IL-7	Peprotech	Cat#217-17
Recombinant human IL-2	Peprotech	Cat#200-02
Mouse PBS-57 CD1d-APC tetramer	NIH Tetramer Core Facility	N/A
Collagenase, type 4	Worthington Biochemical	Cat#LS004186
DNase 1	Sigma-Aldrich	Cat#DN25
ACK lysing buffer	Thermo Fisher	Cat#A1049201
SYTOX Green	Thermo Fisher	Cat#S34860
YOYO-1	Thermo Fisher	Cat#Y3601
Annexin V Alexa Fluor 488	Thermo Fisher	Cat#A13201
Annexin V Alexa Fluor 647	Thermo Fisher	Cat#A23204
Annexin V APC	Biolegend	Cat#640941
SiR-DNA	Cytoskeleton, Inc	Cat#CY-SC007
FluoroBrite DMEM	Thermo Fisher	Cat#A1896702
Opti-MEM	Thermo Fisher	Cat#11058021
Poly-D-Lysine	Sigma-Aldrich	Cat#A-003-E
Glycine	Sigma-Aldrich	Cat#G7126
CellTrace Violet	Thermo Fisher	Cat#C34557
Zombie Green Fixable Viability Dye	Biolegend	Cat#423112
Dynabeads MyOne Streptavidin T1	Thermo Fisher	Cat#65601
Trichloroacetic acid	Sigma-Aldrich	Cat#91228
ActinGreen-488	Thermo Fisher	Cat#R37110
Hoechst 33342	Thermo Fisher	Cat#H3570
SlowFade Diamond Antifade Mountant	Thermo Fisher	Cat#S36963
Brain Heart Infusion broth	Anaerobe Systems	Cat#AS-872
Ficoll-Paque PLUS	GE Lifesciences	Cat#17144003
Critical Commercial Assays		
Mouse IL-1β ELISA kit	Thermo Fisher	Cat#88-7013-77; RRID:AB_2574944
Mouse IFNγ ELISA kit	Thermo Fisher	Cat#88-7314-77; RRID:AB_2575068
Human IL-1β ELISA kit	Thermo Fisher	Cat#88-7261-88; RRID:AB_2575054
Pierce™ LDH cytotoxicity assay	Thermo Fisher	Cat#88954
Anti-mouse CD11c microbeads, ultrapure	Miltenyi Biotec	Cat#130-108-338
Mouse Pan T Cell Isolation Kit II	Miltenyi Biotec	Cat#130-095-130
Anti-APC microbeads	Miltenyi Biotec	Cat#130-090-855
Anti-human CD14 microbeads, ultrapure	Miltenyi Biotec	Cat#130-118-906
Pierce BCA Protein Assay	Thermo Fisher	Cat#23227
eBioscience Intracellular Fixation & Permeabilization Buffer Set	Thermo Fisher	Cat#88-8824-00
Click-iT Plus TUNEL Assay, Alexa Fluor 647 dye	ThermoFisher	Cat#C10619

(*Continued on next page*)

Continued		
REAGENT or RESOURCE	SOURCE	IDENTIFIER
Deposited Data		
ImmGen Consortium	Heng et al., 2008	https://www.immgen.org
Experimental Models: Cell Lines		
Primary murine splenic iNKT cell line	This paper	N/A
Primary human iNKT cell clone J24L.17	Brigl et al., 2006	N/A
Experimental Models: Organisms/Strains		
Mouse: *Fas*$^{-/-}$: B6.MRL-*Fas*^{lpr}/J	Jackson Laboratories	JAX stock #000482
Mouse: *Caspase1/11*$^{-/-}$: B6N.129S2-*Casp1*^{tm1Flv}/J	Jackson Laboratories	JAX stock #016621
Mouse: *CD1d*$^{-/-}$	Exley et al., 2003	N/A
Mouse: *Caspase-8*$^{DA/DA}$	Philip et al., 2016	N/A
Mouse: *Gsdmd*$^{-/-}$	Kambara et al., 2018	N/A
Mouse: *Ripk3*$^{-/-}$	Newton et al., 2004	N/A
Mouse: *Mlkl*$^{-/-}$	Murphy et al., 2013	N/A
Mouse: *Ripk3*$^{-/-}$*Casp8*$^{-/-}$	Kaiser et al., 2011	N/A
Mouse: *Gsdme*$^{-/-}$: C57BL/6N-*Gsdme*^{em1Fsha}/J	Jackson Laboratories	JAX stock #032411
Mouse: *Gsdmd*$^{-/-}$*Gsdme*$^{-/-}$	Chen et al., 2019	N/A
Mouse: *Asc*$^{-/-}$	Ozören et al., 2006	N/A
Mouse: WT: C57BL/6NJ (control for *Gsdme*$^{-/-}$ mice)	Jackson Laboratories	JAX stock #005304
Mouse: WT: C57BL/6	Jackson Laboratories	JAX stock #000664
Mouse: *Nlrp3*$^{-/-}$: B6.129S6-*Nlrp3*^{tm1Bhk}/J	Jackson Laboratories	JAX stock #021302
Software and Algorithms		
FlowJo (v10.5.3)	BD Biosciences	https://www.flowjo.com/
R (v3.3.2)	R Foundation for Statistical Computing	http://www.R-project.org
Fiji / ImageJ version 2.0.0	Fiji contributors / ImageJ developers	https://imagej.net/Fiji
Zen (v2.3)	Zeiss	https://www.zeiss.com/microscopy/us/products/microscope-software/zen.html
MetaXpress (v6.0)	Molecular Devices	https://www.moleculardevices.com/products/cellular-imaging-systems/acquisition-and-analysis-software/metaxpress
GraphPad Prism 7	GraphPad Software	https://www.graphpad.com/
Multiplot Studio v2	GenePattern, Broad Institute	https://www.genepattern.org/
Other		
96-well plate | No. 1.5 Coverslip | 5 mm Glass Diameter | Poly-D-Lysine Coated	MatTek Corporation	Cat#P96GC-1.5-5-F
Greiner Bio-One SensoPlate 96-Well Glass Bottom Microplates	Greiner Bio-One	Cat#655892

LEAD CONTACT AND MATERIALS AVAILABILITY

Further information and requests for resources and reagents should be directed and will be fulfilled by the Lead Contact, Michael B. Brenner (mbrenner@research.bwh.harvard.edu). This study did not generate new unique reagents.

EXPERIMENTAL MODEL AND SUBJECT DETAILS

Mice

Wild-type C57BL/6J, *Caspase1/11*$^{-/-}$ (Kuida et al., 1995), *Nlrp3*$^{-/-}$ (Kovarova et al., 2012), *Fas*$^{-/-}$, and *CD1d*$^{-/-}$ (Exley et al., 2003) mice were purchased from Jackson Laboratories and were housed under specific pathogen-free conditions at the Center for Comparative Medicine at Brigham and Women's Hospital (BWH). All procedures were approved by the BWH Institutional Animal Care and Use Committee. Mice were euthanized by CO_2 asphyxiation followed by cervical dislocation in accordance to the BWH IACUC guidelines. Bone marrow from the following mice were kindly provided by the following

investigators: *Caspase-8*$^{DA/DA}$ (Philip et al., 2016) was provided by Dr. Igor Brodsky, *Gsdmd*$^{-/-}$ (Kambara et al., 2018) was provided by Dr. Hongbo Luo, *Ripk3*$^{-/-}$ (Newton et al., 2004) and *Mlkl*$^{-/-}$ (Murphy et al., 2013) were provided by Dr. Ben Croker, *Ripk3*$^{-/-}$*Casp8*$^{-/-}$ (Kaiser et al., 2011) was provided by Dr. Edward Mocarski, *Gsdme*$^{-/-}$ and *Gsdmd*$^{-/-}$*Gsdme*$^{-/-}$ (Chen et al., 2019) were provided by Dr. Petr Broz, and *Asc*$^{-/-}$ (Ozören et al., 2006) was provided by Dr. Gabriel Nuñez.

Bacterial strains and growth

B. fragilis (NCTC 9343, a kind gift from Dr. Laurie Comstock) was grown anaerobically at 37°C in Brain Heart Infusion broth (Anaerobe Systems). The culture's optical density at 600 nm was measured to determine the colony-forming units. *C. trachomatis* serovar D (UW-3/Cx; ATCC, kindly provided by Dr. Michael Starnbach) was propagated within McCoy cells grown in RPMI 1640 (Thermo Fisher) supplemented with 10% FBS, 2 mM L-glutamine, 0.1 mM nonessential amino acids and 1 mM sodium pyruvate. Cells were lysed with sterile glass beads followed by sonication to release bacteria from the inclusion. Elementary bodies (EBs) were purified by density gradient centrifugation, aliquoted and stored at −80°C in medium containing 220 mM sucrose, 15 mM sodium phosphate, 4 mM potassium phosphate and 5 mM L-glutamic acid. Aliquots were thawed immediately before use. Inclusion forming units (IFUs) of thawed EBs were tittered on McCoy cell monolayers.

Human samples

All human samples were used with approval from the Brigham and Women's Hospital Institutional Review Board. As a source of human peripheral blood mononuclear cells (PBMCs), leukoreduction filters were obtained from the Brigham and Women's Hospital Kraft Family Blood Donor Center. Human iNKT cells were derived from healthy donor peripheral blood as previously described (Brigl et al., 2006).

METHOD DETAILS

Preparation of murine bone marrow-derived dendritic cells (BMDCs)

To generate BMDCs, the femoral and tibial bones of 6-15-week old female mice were flushed with RPMI media (Thermo Fisher) and the bone marrow suspension was passed through a 40 μm cell strainer. The filtered bone marrow cells were depleted of red blood cells (RBCs) following a 1-minute treatment with ACK lysing buffer (Thermo Fisher) on ice. 4x10^6 bone marrow cells per untreated 10-cm dish were cultured in 10 mL of IMDM medium (Thermo Fisher) supplemented with 10% heat-inactivated fetal bovine serum (Gemini Bio-Products), 2 mM L-glutamine, 100 U/ml penicillin / 100 μg/ml streptomycin, 25 mM HEPES, 50 μM β-mercaptoethanol (all Thermo Fisher), and 20 ng/ml of recombinant murine GM-CSF (Peprotech) and kept in a humidified incubator at 37°C with 5% CO_2. An additional 10 mL of media was added to plates on day 4 of differentiation. After 7 days of differentiation, the non-adherent cells in the culture supernatant and loosely adherent cells harvested by gentle washing with 2 mM EDTA (Thermo Fisher) in HBSS (Thermo Fisher) were pooled and used as the starting source of cells for most experiments. For all microscopy-based experiments, the CD11c$^+$ fraction was enriched to 99% purity by incubating the starting population with CD11c microbeads (Miltenyi Biotec) and passing them sequentially through two LS columns (Miltenyi Biotec).

Preparation of human monocyte-derived macrophages (MDMs)

PBMCs were isolated using Ficoll-Paque PLUS (GE Lifesciences) according to the manufacturer's instructions. To prepare MDMs, CD14$^+$ cells were isolated using CD14 microbeads (Miltenyi Biotec). CD14$^+$ cells were plated in 6-well plates at 3x10^6 cells per well in 3 mL of RPMI medium (Thermo Fisher) supplemented with 10% heat-inactivated fetal bovine serum, 2 mM L-glutamine, 100 U/ml penicillin / 100 μg/ml streptomycin, 25 mM HEPES, 50 μM β-mercaptoethanol, and 100 ng/ml of recombinant human GM-CSF (Peprotech) and kept in a humidified incubator at 37°C with 5% CO_2. An additional 3 mL of media was added to wells on day 3 of differentiation. After 6 days of differentiation, the non-adherent cells in the culture supernatant and the loosely adherent cells lifted by gentle use of a cell scraper were pooled and used as the starting source of cells for experiments.

Generation of iNKT cell lines

Murine iNKT cells were enriched from the spleens of female C57BL/6J mice as previously described (Chiba et al., 2009). Briefly, splenocytes were harvested from female C57BL/6J mice by pressing spleens through a 40-μm cell strainer, followed by 1-minute treatment with ACK lysis buffer on ice to deplete RBCs. T cells were negatively selected using the Pan T Isolation Kit II following the manufacturer's protocol (Miltenyi Biotec). iNKT cells were labeled with APC-conjugated CD1d tetramer loaded with PBS-57 lipid antigen (National Institutes of Health Tetramer Core Facility) and iNKT cells were enriched using anti-APC beads (Miltenyi Biotec). To prepare APCs for expansion of iNKT cells, CD11c$^+$ splenocytes were enriched by pressing spleens of female C57BL/6J mice through a 40-μm cell strainer followed by digestion in DMEM (Thermo Fisher) containing 10% FBS, collagenase type IV (Worthington Biochemical, 1 mg/ml), and DNase1 (Sigma, 20 μg/ml) for 30 minutes at 37°C. Splenocytes were depleted of RBCs following a 1-minute treatment with ACK lysis buffer on ice. CD11c$^+$ splenocytes were positively selected using CD11c microbeads following the manufacturer's protocol. CD11c$^+$ splenocytes were irradiated, plated at 2x10^5 cells per well in 24 well plates and were loaded with αGalCer (50 ng/ml) for 6 hours. 2x10^6 freshly isolated iNKT cells were added per well in 24-well plates (1:10 ratio of CD11c$^+$ splenocytes to iNKT cells) in complete RPMI medium containing 10% FBS. Two days later, IL-2 (Peprotech, 0.5 ng/ml) and IL-7 (Peprotech,

10 ng/ml) were added to the media. 21 days following the start of the expansion, iNKT cells were enriched to 99% purity by FACS-sorting using APC-conjugated CD1d tetramer loaded with PBS-57 lipid antigen (NIH Tetramer Core Facility, 1:500) and an antibody against the TCR β chain (Biolegend, 1:200). iNKT cells were then stimulated with freshly-isolated $CD11c^+$ splenocytes as described above and were frozen 21 days later for use in experiments. The human iNKT cell clone J24L.17 was previously generated from healthy donor peripheral blood as described (Brigl et al., 2006). Briefly, iNKT cells sorted using APC-conjugated CD1d tetramer loaded with PBS-57 lipid antigen (1:500) were cultured at 37°C with 5% CO2 in RPMI culture medium containing 10% FBS, 2% human AB serum, 1% penicillin and streptomycin, and 1% L-glutamine in the presence of irradiated allogeneic PBMCs and PHA. After 5–10 days of culture, 200 U/ml recombinant human IL-2 (Peprotech) was added to the medium.

Cell stimulation

Where indicated, BMDCs were primed with P3C (Invivogen, 0.5 μg/ml) prior to addition of inflammasome agonists, iNKT cells, or recombinant, hexameric FasL (rFasL or MegaFasL, Adipogen, 0.1 μg/ml). The following stimulation conditions apply for ELISAs, LDH release assays, and flow cytometry-based assays. For inflammasome activation controls, BMDCs were primed for 4 hours and treated with monosodium urate (MSU) crystals (Invivogen, 100 μg/ml) for 6 hours or nigericin (Invivogen, 10 μM) for 1 hour. BMDCs were primed for 24 hours in the presence or absence of αGalCer (generously provided by Dr. Gurdyal Besra, 50 ng/ml) prior to addition of iNKT cells or rFasL. BMDCs were routinely plated at $5x10^4$ cells per well in 96-well plates for ELISAs, LDH release assays, and flow cytometry-based assays. For immunoblots, BMDCs were plated in 6-well plates at $1.25x10^6$ cells per well. For microscopy, BMDCs were plated in glass-bottom 96-well plates at $2x10^4$ cells per well. A 4:1 ratio of iNKT cells to BMDCs was used for co-culture assays. For experiments with human cells, MDMs were primed with P3C (2 μg/ml) for 24 hours in the presence or absence of αGalCer (50 ng/ml) prior to addition of iNKT cells, rFasL, or nigericin. MDMs were cultured in the presence of iNKT cells or rFasL for 24 hours, and were stimulated with nigericin for 2 hours. The human iNKT cell line J24L.17 has been previously described (Brigl et al., 2006) and was used for the co-culture experiments. $5x10^4$ MDMs and $2x10^5$ human iNKT cells were used per condition for co-culture experiments. Antibody-mediated neutralization experiments were performed in the presence of a FasL-blocking antibody (clones MFL3 and NOK-1 for murine and human studies, respectively, both from Biolegend) or an isotype control (clones HTK888 and MOPC-21 for murine and human studies, respectively, both from Biolegend) at 10 ug/ml. All stimulations were performed in complete RPMI medium containing 10% FBS.

ELISAs and LDH release assays

At the indicated time points, cell-free supernatants were harvested by spinning the plates twice at 400 x g for 5 minutes, serially, while transferring to new plates. Quantification of secreted murine IL-1β and IFNγ was performed using ELISA kits from Thermo Fisher according to the manufacturer's protocol. For LDH release assays, fresh cell-free supernatants were assayed at the indicated time points using the Pierce LDH cytotoxicity assay kit based on the manufacturer's instructions. LDH release is depicted as percentage of maximum death (cells treated with 0.1% Triton X-100). The percentage of LDH was calculated as follows: LDH (% of Maximum): (sample LDH – background LDH) / (max LDH – background LDH in the presence of lysis buffer)

Flow Cytometric Analysis of FasL Expression

iNKT cells were labeled with 0.5 μM CellTrace Violet (Thermo Fisher) in HBSS for 30 minutes at 37°C. They were spun down at 300 x g for 10 minutes and any remaining CellTrace Violet was quenched by incubating the iNKT cells in complete RPMI for 5 minutes. iNKT cells were co-cultured with unlabeled BMDCs in 96-well plates at a ratio of 4:1 and the cells were harvested by gentle pipetting after the indicated time points. Cells were washed 2X in PBS and dead cell exclusion was performed by staining cells in PBS with Zombie Green live/dead dye (Biolegend, 1:500) for 30 minutes on ice. Following two washes in FACS buffer, cells were incubated with an Fc receptor-blocking antibody (16-0161-86, Thermo Fisher) for 15 minutes on ice. For assessment of surface FasL expression, cells were stained with a PE-conjugated antibody against FasL (MFL3, Thermo Fisher, 1:50) for 30 minutes at room temperature. During the last 15 minutes of the incubation, an antibody against PE (PE001, Biolegend, 1:25) was added to amplify the signal of the PE-conjugated anti-FasL antibody. Cells were washed twice in FACS buffer and were immediately analyzed by flow cytometry using an LSRFortessa (BD Biosciences). To assess the expression of intracellular (or whole cell) FasL, iNKT cells were stained with APC-conjugated PBS-57 CD1d tetramer, fixed, and permeabilized using the eBioscience intracellular fixation and permeabilization kit (Thermo Fisher) according to the manufacturer's instructions, followed by staining with PE-conjugated anti-FasL (MFL3, Thermo Fisher, 1:50). The mean fluorescence intensity values reflecting FasL expression on iNKT cells were quantified using FlowJo software (BD Biosciences) by gating on the live, CellTrace Violet-positive cells (for cell surface FasL) or by gating on the live, PBS-57 CD1d tetramer positive cells (for intracellular or whole-cell staining).

Immunoblotting

For co-culture experiments, BMDCs were primed and co-cultured with iNKT cells in complete RPMI medium containing 10% FBS. Cell-free supernatants were transferred to 2 mL Eppendorf Safe-Lock tubes and extracellular IL-1β was immunoprecipitated by rotating the tubes overnight at 4°C in the presence of 0.5 μg of biotinylated polyclonal goat anti-mouse IL-1β (BAF-401, R&D) and 200 μg of Dynabeads MyOne Streptavidin T1 magnetic beads (Thermo Fisher). For experiments were BMDCs were stimulated with rFasL (and corresponding untreated and nigericin-treated controls), BMDCs were washed 3x with ice-cold PBS after priming,

switched to serum-free Opti-MEM media, and the cell-free supernatants were precipitated with 10% Trichloroacetic acid (TCA, Sigma) after the indicated time points. Cell lysates were prepared by lysing cells in RIPA buffer supplemented with cOmplete protease inhibitor cocktail (Roche), and the concentrations of the lysates were quantified using the Pierce BCA protein assay kit (Thermo Fisher). Cell lysates, supernatants, and immunoprecipitated IL-1β were separated by SDS-PAGE on 12% Mini-PROTEAN TGX or Criterion TGX gels (Bio-Rad) and transferred onto 0.2 μm PVDF membranes using a Trans-Blot Turbo transfer system (Bio-Rad). Membranes were blocked with 5% nonfat dry milk containing 0.1% Tween 20 in TBST for 1 hour at room temperature, and then incubated with primary antibodies overnight at 4C unless noted otherwise. The following were the primary antibodies used: Actin (Sigma, A5441, 1:10000), IL-1β (R&D, AF-401, 1:800), IL-1β (Genetex, GTX74034, 1:1000, used to probe immunoprecipitated IL-1β), caspase-1 (Adipogen, AG-20B-0042-C100, 1:1000), caspase-8 (Enzo, ALX-804-447-C100, 1:1000), cleaved caspase-8 (Cell Signaling, 8592, 1:1000), caspase-3 (Cell Signaling, 9662, 1:1000), cleaved caspase-3 (Cell Signaling, 9661, 1:1000), FLIP (Cell Signaling, 56343, 1:1000), caspase-6 (Cell Signaling, 9762, 1:1000), caspase-7 (Cell Signaling, 12827, 1:1000), caspase-9 (Cell Signaling, 9508, 1:1000), GSDMD (Abcam, ab209845, 1:1000), GSDME (Abcam, ab215191, 1:1000, incubation performed at room temperature for 1.5 hours). Membranes were incubated with the following horseradish peroxidase-conjugated secondary antibodies at a 1:10000 dilution for 1 hour at room temperature: goat anti-mouse IgG (115-035-146), donkey anti-rabbit IgG (711-035-152), bovine anti-goat IgG (805-035-180), and donkey anti-rat IgG (712-035-150), all from Jackson Immunoresearch. Membranes were developed using Clarity Western ECL (Bio-Rad) and imaged using a ChemiDoc Touch MP (Bio-Rad).

Flow Cytometric Quantification of Cell Death

To distinguish early apoptosis from necrosis, BMDCs were stimulated on non-treated 96-well plates. After the indicated time points, the supernatants were removed and the cells were incubated in 5 mM EDTA in HBSS for 5 minutes at 37°C. BMDCs were harvested from the plate by gentle pipetting, transferred to 96-well V-bottom plates, and washed twice in FACS buffer (Fluorobrite DMEM supplemented with 5% FBS, 25 mM HEPES, and 2 mM EDTA). BMDCs were incubated with an Fc receptor-blocking antibody (16-0161-86, Thermo Fisher) for 15 minutes prior to staining with antibodies against CD11c (N418, Thermo Fisher, 1:300) and MHC-II (M5/114.15.2, Thermo Fisher, 1:400) for 30 minutes on ice. Cells were then washed twice, once in FACS buffer followed by another wash in annexin V binding buffer (Biolegend). BMDCs were then stained with annexin V-APC (Biolegend, 1:50) and Sytox Green (Thermo Fisher, 50 nM) in 100 μL for 5 minutes on ice after which they were diluted to 300 μL with annexin V binding buffer. $CD11c^+$ BMDCs staining positive or negative for annexin V and Sytox Green were immediately analyzed immediately by flow cytometry using an LSRFortessa and the percentages of differently labeled cells were calculated using FlowJo software. For co-culture experiments, iNKT cells were labeled with 0.5 μM CellTrace Violet prior to co-culture with BMDCs, and the CellTrace Violet-negative, $CD11c^+$ BMDCs were gated on for the flow cytometric analysis of cell death.

Live Imaging of Cell Death

Dead cells were depleted from BMDCs using a dead cell removal kit (Miltenyi Biotec) and $CD11c^+$ BMDCs were subsequently enriched to 99% purity by incubating the live fraction with CD11c microbeads following the manufacturer's instructions. $CD11c^+$ BMDCs were plated on 96-well glass bottom plates (Greiner Bio-One) coated with Poly-D-Lysine (Sigma, 0.5 mg/ml in 0.1 M borate buffer) in complete Fluorobrite DMEM (Thermo Fisher) supplemented with 2.5 mM $CaCl_2$ (Sigma). $CD11c^+$ BMDCs were primed for 6 or 24 hours prior to stimulation with nigericin or rFasL, respectively. To visualize phosphatidylserine exposure and membrane permeabilization by time-lapse microscopy, Annexin V-AF647 (Thermo Fisher) or Annexin V-AF488 (Thermo Fisher) were added into the media at 1:50 and YOYO-1 (Thermo Fisher) was added at 250 nM for the duration of the stimulation. To track the nuclear DNA over time, the live $CD11c^+$ BMDCs were enriched as mentioned above and were labeled with 0.25 μM SiR-DNA (Cytoskeleton, Inc) for 6 hours prior to stimulation with nigericin or rFasL. Cells were washed three times with complete Fluorobrite DMEM media and YOYO-1 was added at 250 nM for the duration of the stimulation. Cells were then stimulated with nigericin or rFasL and were immediately visualized by time-lapse widefield microscopy. Images were acquired every 5 minutes for 4 – 6 hours.

Time-lapse widefield microscopy was performed using a Molecular Devices ImageXpress Micro Confocal that was maintained at 37C and 5% CO2 for the duration of the stimulation. Images were acquired using a 40X Plan Apo objective and analyzed using MetaXpress software. A Zeiss LSM 800 confocal microscope equipped with a 63X Plan Apo oil objective and an incubation chamber maintained at 37C and 5% CO_2 was also used. Images were analyzed using Zen 2.3 software (Zeiss). Final image analysis was performed using ImageJ software (NIH).

TUNEL staining

BMDCs were plated on 96-well glass bottom, Poly-D-Lysine-coated plates (MatTek) coated with Poly-D-Lysine in complete RPMI media. BMDCs were primed for 6 and 24 hours prior to stimulation with nigericin and rFasL, respectively. Following 1 or 6 hour stimulation with nigericin or rFasL, respectively, the supernatant was removed and the cells were immediately fixed with 4% paraformaldehyde for 30 minutes at room temperature. The fixative was then removed, and the cells were permeabilized (0.25% Triton X-100 in PBS) for 20 minutes at room temperature. After two washes with deionized water, the cells were stained with a Click-iT Plus TUNEL Assay kit (Thermo Fisher) according to the manufacturer's instructions. Following completion of TUNEL staining, the cells were stained with ActinGreen (Thermo Fisher) as suggested by the manufacturer. The cells were then stained with 5 μg/ml Hoechst 33342 (Thermo Fisher) for 15 minutes at room temperature. After two PBS washes, the cells were mounted with SlowFade Diamond

Antifade Mountant (Thermo Fisher). The samples were imaged using a Zeiss LSM 800 confocal microscope equipped with a 20X Plan Apo oil objective. Images were analyzed using Zen 2.3 software. Final image analysis was performed using ImageJ software.

Cell Sorting

BMDCs differentiated from the bone marrow of five C57BL/6J mice were pooled and sorted on a BD FACS Aria (BD Biosciences). Briefly, BMDCs were harvested, pooled, incubated with Fc receptor-blocking antibody (16-0161-86, Thermo Fisher) for 15 minutes on ice, and the $CD11c^+$ BMDCs were enriched using CD11c microbeads following the manufacturer's instructions. To sort GM-DCs and GM-Macs, the CD11c-enriched BMDCs were stained with antibodies against CD11c (N418, Thermo Fisher, 1:300), CD11b (M1/70, Thermo Fisher, 1:300) MHC-II (M5/114.15.2, Thermo Fisher, 1:400), CD115 (AFS98, Biolegend, 1:100), MerTK (DS5MMER, Thermo Fisher, 1:100), and CD135 (A2F10, Biolegend, 1:50). GM-Macs were sorted as $CD11c^+CD11b^{hi}MHCII^{lo\text{-}int}CD115^+MerTK^+$ while GM-DCs were sorted as $CD11c^+CD11b^{int}MHCII^{hi}CD115^-CD135^+$ (see also Figure S1). Dead cells were excluded with PI.

Bacterial Infections

BMDCs were plated in 96-well plates at $5x10^4$ cells per well and were incubated with log-phase *B. fragilis* (NCTC 9343) at multiplicities of infection (MOIs) of 10, 20, 40, and 80. Plates were spun at 300 x g for 5 minutes and incubated for 3 hours at 37°C to allow uptake of *B. fragilis* by BMDCs. The cells were then washed 2x with complete RPMI and were allowed to rest for 21 hours to complete 24 hours of exposure to priming stimulus provided by *B. fragilis*. For infections with *C. trachomatis* serovar D (UW-3/Cx; ATCC), BMDCs were plated as described above and infected by adding *C. trachomatis* at inclusion forming units (IFUs) of 1.5 and 3 and spinning the plates at 37°C for 1 hour. BMDCs were then incubated at 37°C for another 3 hours. Following 4 hours of infection, BMDCs were washed 3x with complete RPMI and were allowed to rest for 20 hours to complete 24 hours of exposure to priming stimulus provided by *C. trachomatis.* 24 hours after BMDCs were first exposed to *B. fragilis* or *C. trachomatis*, a monoclonal antibody that blocks FasL (MFL3, Biolegend, 20 μg/ml) or an isotype control (HTK888, Biolegend, 20 μg/ml) was added to BMDCs, followed by addition of iNKT cells at a 1:1 ratio. Plates were spun at 300 x g for 5 minutes and were incubated at 37°C 24 hours prior to analysis of the cell-free supernatants by ELISA.

ImmGen expression data

Expression data for iNKT and T cell populations is publicly available at https://www.ncbi.nlm.nih.gov/geo/query/acc.cgi?acc=GSE15907 or http://www.immgen.org.

To identify surface-expressed proteins, population mean expression data was first filtered to include genes within Gene Ontology (http://geneontology.org/) term ''cell surface'' GO0009986 with an expression cutoff of greater than 120 units (Cohen et al., 2013). Multiplot Studio was used to generate the expression-expression plot in Figure 2B (GenePattern, Broad Institute).

QUANTIFICATION AND STATISTICAL ANALYSIS

Data are presented as mean ± standard deviation (SD) as indicated in the figure legends and were analyzed in GraphPad Prism 7. Statistical analyses were performed in R using Student's unpaired t test as indicated in the legends. Significance is depicted with asterisks on graphs as follows: *$p < 0.05$, **$p < 0.01$, ***$p < 0.001$, ****$p < 0.0001$.

DATA AND CODE AVAILABILITY

This study did not generate any unique datasets or code.

Cell Reports, Volume *31*

Supplemental Information

A Two-Cell Model for IL-1β Release Mediated by Death-Receptor Signaling

Carlos A. Donado, Anh B. Cao, Daimon P. Simmons, Ben A. Croker, Patrick J. Brennan, and Michael B. Brenner

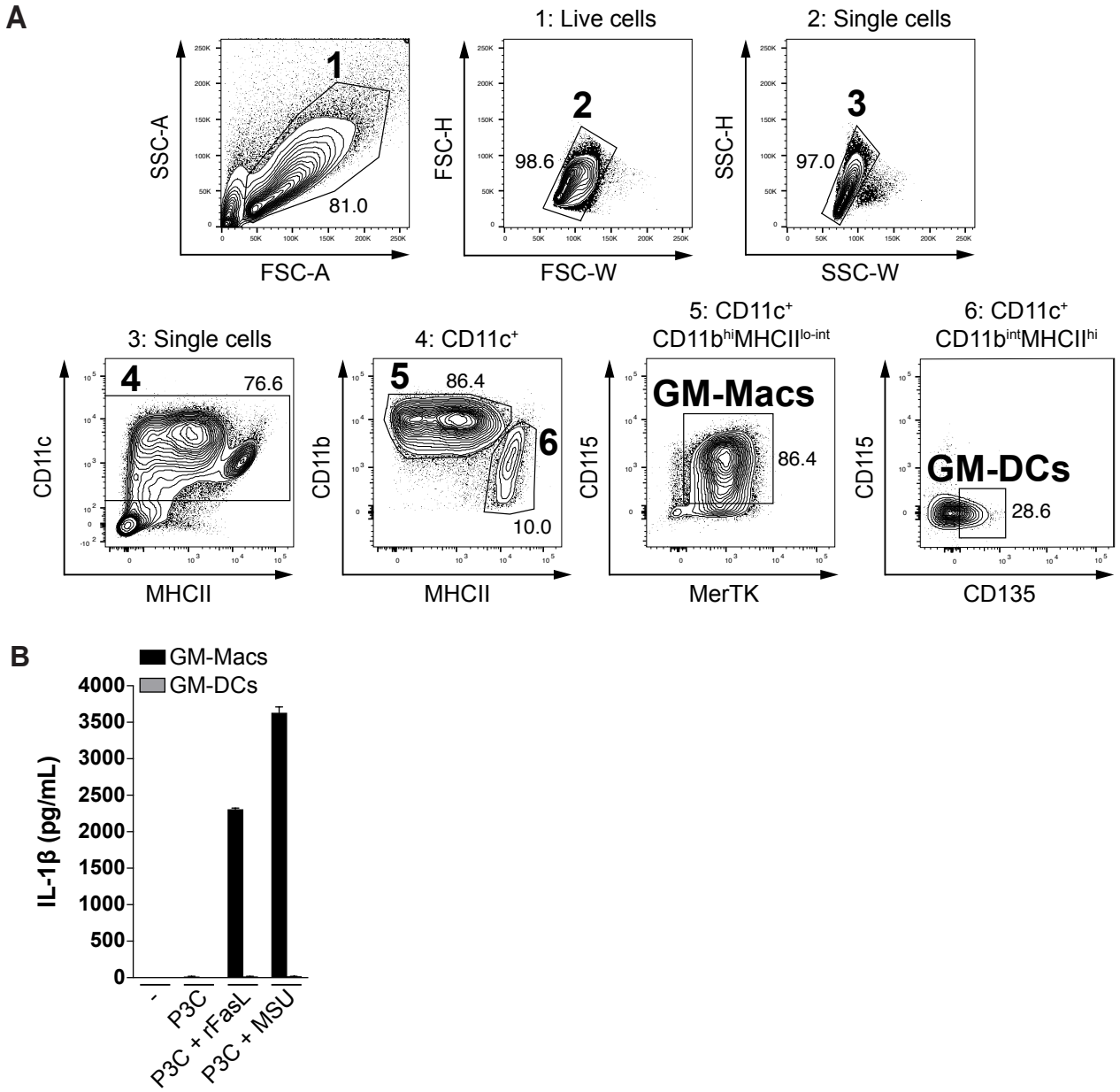

Figure S1 (related to Figure 2): Monocyte-derived Macrophages and not DCs are Responsible for FasL-induced IL-1β Release in GM-CSF Mouse Bone Marrow Cultures

(A) Representative flow cytometry plots demonstrating the gating strategy utilized to FACS-sort GM-Macs (GM-CSF monocyte-derived macrophages, $CD11c^{+}CD11b^{hi}MHCII^{lo\text{-}int}CD115^{+}MerTK^{+}$) and GM-DCs (GM-CSF-derived DCs, $CD11c^{+}CD11b^{int}MHCII^{hi}CD115^{-}CD135^{+}$) from mouse bone marrow cultures grown for 7 days in GM-CSF-containing media. Boxes depict gates (labeled with large, bold text) and the small numbers correspond to percentage of cells in each gate. The parent gates are labeled at the top of each plot.

(B) GM-Macs and GM-DCs were FACS-sorted from seven-day GM-CSF bone marrow cultures and were left untreated or primed with P3C for 6 hours prior to stimulation with rFasL for 24 hours. IL-1β release was quantified by ELISA. MSU-treated P3C-primed GM-Macs or GM-DCs were used as a control.

Error bars represent mean + SD of triplicate samples. Each panel is representative of two different experiments.

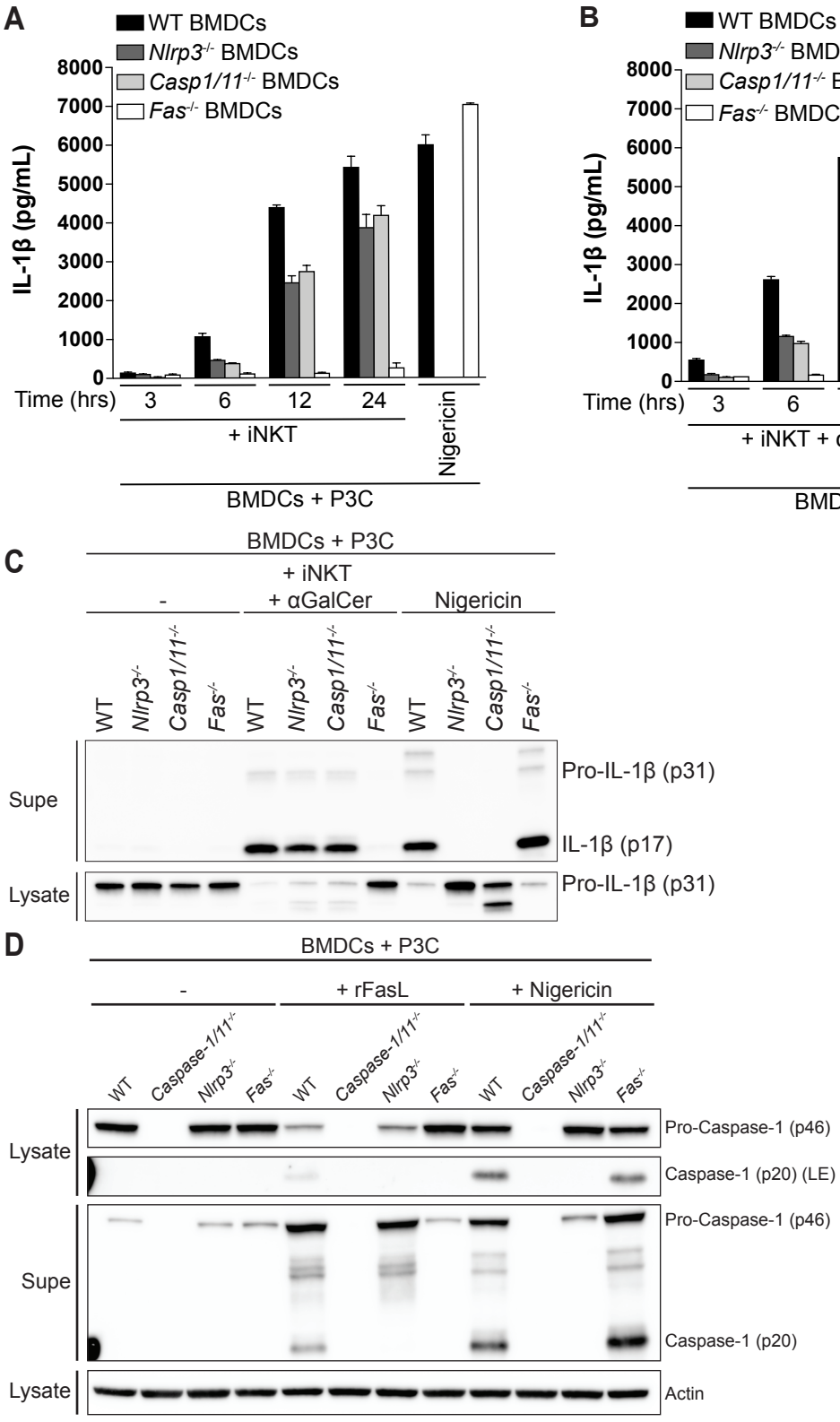

Figure S2 (related to Figure 3): Fas Ligation Elicits Inflammasome-dependent and -independent IL-1β Release by TLR-Primed BMDCs

(A-C) P3C-primed BMDCs from WT, *Nlrp3*$^{-/-}$, *Caspase1/11*$^{-/-}$ and *Fas*$^{-/-}$ mice were cultured alone or with iNKT cells for (A and B) the indicated times or (C) 12 hours in the (A) absence or (B and C) presence of αGalCer. (A and B) IL-1β release was quantified by ELISA and (C) cell-associated and extracellular IL-1β were analyzed by immunoblot. Nigericin-treated BMDCs were used as a control.

(D) P3C-primed BMDCs from WT, *Nlrp3*$^{-/-}$, *Caspase1/11*$^{-/-}$ and *Fas*$^{-/-}$ mice were stimulated with rFasL for 6 hours and the cell lysates and cell-free supernatants were probed for the indicated proteins by immunoblot.

Error bars represent mean + SD of triplicate samples. Each panel is representative of at least three different experiments.

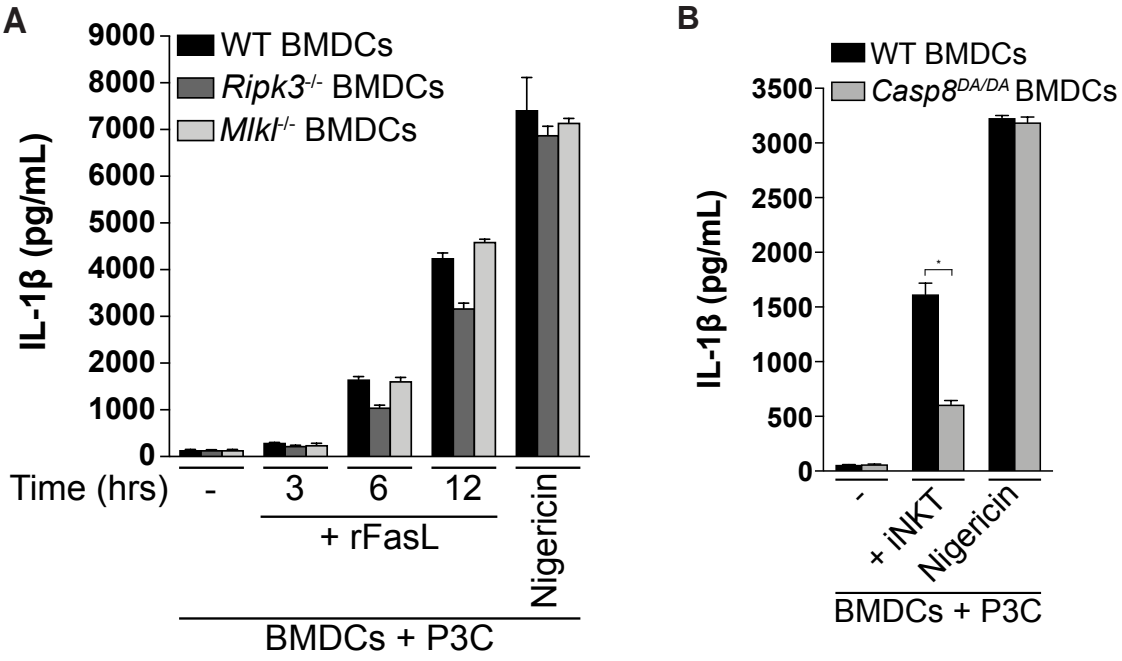

Figure S3 (related to Figure 3): FasL-Induced IL-1β Release by BMDCs Proceeds Independently of Necroptosis and Requires Caspase-8 Self-Cleavage

(A) P3C-primed BMDCs from WT, *Ripk3*$^{-/-}$, and *Mlkl*$^{-/-}$ mice were cultured alone or in the presence of rFasL for the indicated times. IL-1β release was quantified by ELISA. Nigericin-treated BMDCs were used as a control.

(B) P3C-primed BMDCs from WT and *Caspase-8*$^{DA/DA}$ mice were cultured alone or with iNKT cells for 24 hours. IL-1β release was quantified by ELISA.

Error bars represent mean + SD of triplicate samples. Each panel is representative of at least three different experiments. *p <0.05 as determined by Student's unpaired t test.

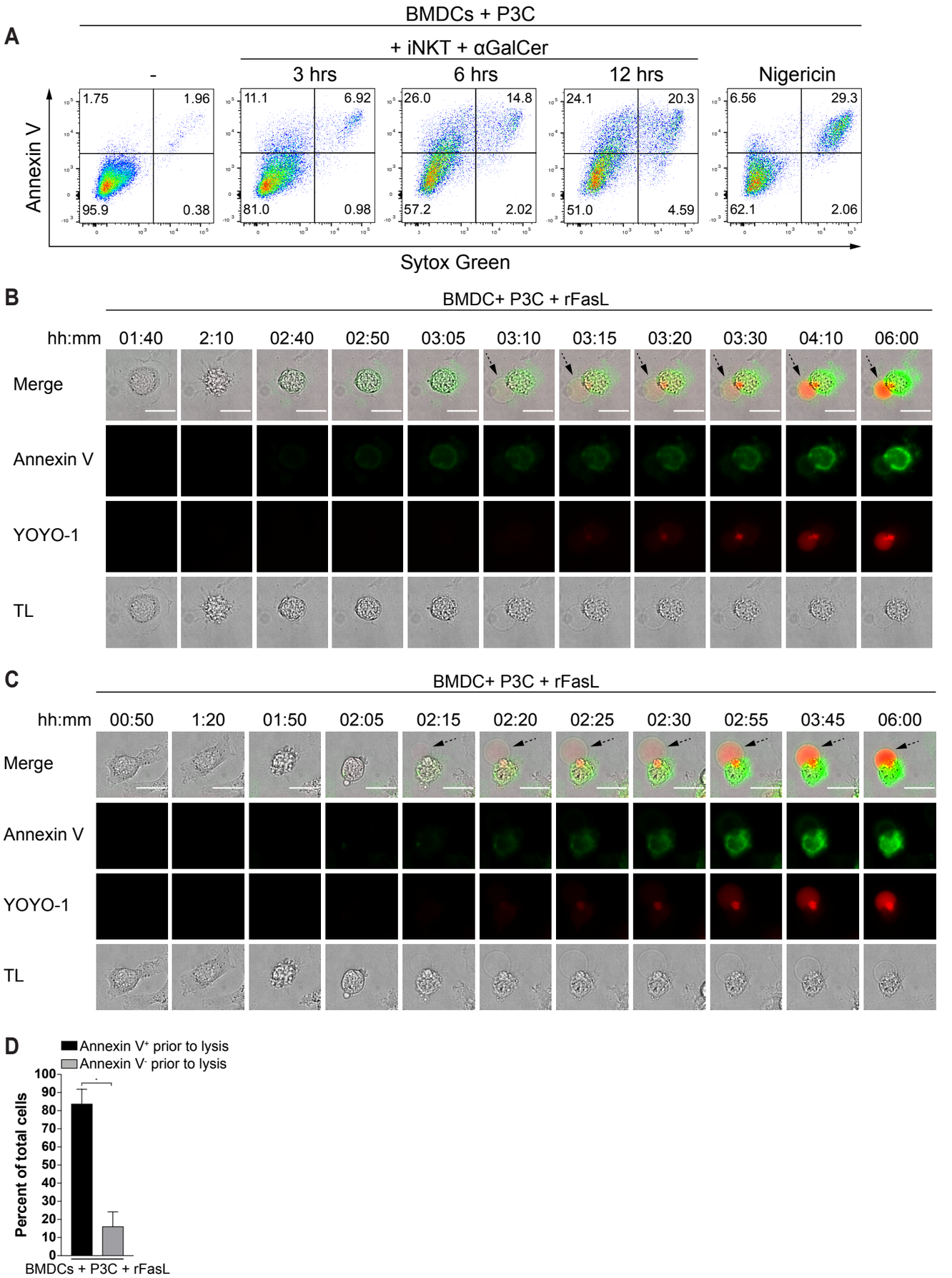

Figure S4 (related to Figure 5): Fas Ligation Elicits Apoptosis that Rapidly Transitions to Necrosis in TLR-primed BMDCs

(A) P3C-primed BMDCs were cultured alone or with CellTrace Violet-labeled iNKT cells in the presence of αGalCer. After the indicated times, the cells were harvested, labeled with Sytox Green and annexin V and the extent of early-apoptotic and necrotic BMDCs was analyzed by gating on the CellTrace Violet-negative, $CD11c^+$ cells. Nigericin-treated BMDCs were used as a control.

(B and C) P3C-primed BMDCs were stimulated with rFasL and morphological changes, annexin V (green) and YOYO-1 (red) staining were monitored by live imaging over 6 hours. Images were captured every 5 minutes and representative timepoints are shown. Dotted arrows point at necrotic plasma membrane balloons. The scale bars represent 10 μm. Note that while the cell in (B) stains with annexin V prior to the formation of necrotic balloons, the cell in (C) becomes annexin V-positive following lysis.

(D) P3C-primed BMDCs were stimulated with rFasL for 6 hours and the number of cells that stained positive for annexin V prior (Annexin V^+ prior to lysis) or concurrently (Annexin V^- prior to lysis) to the formation of necrotic plasma membrane balloons was quantified. A total of 893 cells were counted.

Error bars represent mean + SD of 27 replicate wells from two different experiments. Panels A, B, and C are representative of at least three different experiments. *p <0.05 as determined by Student's unpaired t test.

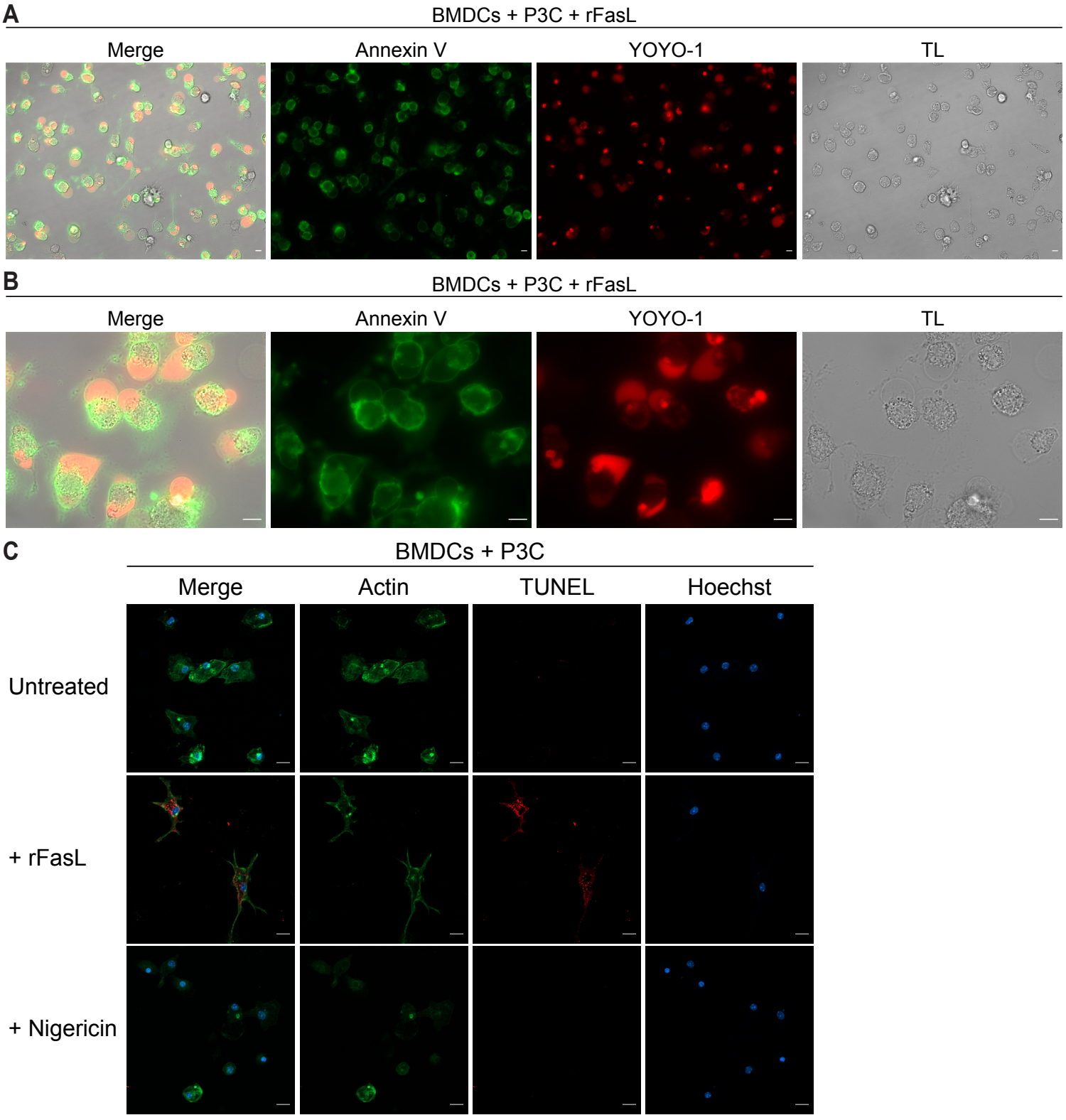

Figure S5 (related to figure 6): Nuclear DNA diffuses to the Cytosol and Necrotic Balloons when Necrosis is Preceded by Apoptosis in TLR-Primed BMDCs

(A and B) P3C-primed BMDCs were stimulated with rFasL and morphological changes (TL), annexin V (green) and YOYO-1 (red) staining were assessed by live imaging after 4 hours. Representative images demonstrate the extent of YOYO-1 diffusion to the cytosol and necrotic plasma membrane balloons following Fas ligation at (A) 20X and (B) 63X magnification. The scale bars represent 10 μm.

(C) P3C-primed BMDCs were left untreated or stimulated with rFasL or nigericin for 6 hours or 1 hour, respectively. TUNEL staining (red) was performed to assess the extent of DNA fragmentation. Actin (green) and nuclear (Hoechst, blue) staining are also shown. The scale bars represent 20 μm.

Each panel is representative of at least three different experiments.

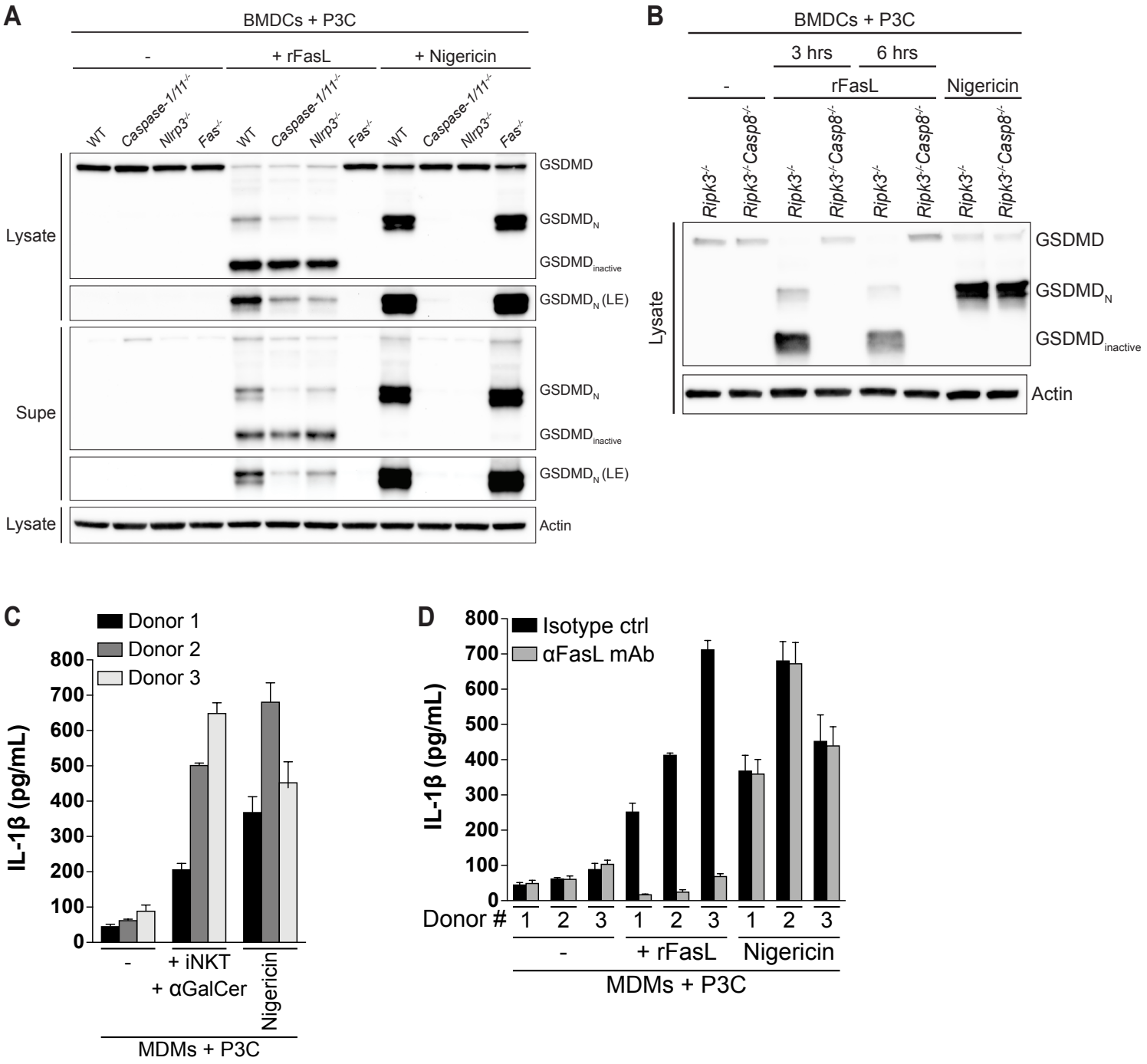

Figure S6 (related to figure 7): Caspase-8 Mediates Inflammasome-independent Cleavage of GSDMD in response to Fas ligation

(A and B) P3C-primed BMDCs from WT, *Nlrp3*$^{-/-}$, *Caspase1/11*$^{-/-}$ and *Fas*$^{-/-}$ mice or (B) *Ripk3*$^{-/-}$ and *Ripk3*$^{-/-}$*Casp8*$^{-/-}$ mice were stimulated with rFasL for (A) 6 hours or (B) the indicated times and the cell lysates and cell-free supernatants were probed for the indicated proteins by immunoblot.

(C) P3C-primed human monocyte-derived macrophages (MDMs) from 3 donors were cultured alone or with iNKT cells for 24 hours in the presence of αGalCer (50 ng/ml). IL-1β release was quantified by ELISA. As a control, MDMs were treated with nigericin (10 μM) for 2 hours.

(D) P3C-primed MDMs from 3 donors were stimulated with rFasL for 24 hours in the presence of a FasL-blocking antibody (αFasL mAb) or an isotype control. IL-1β release was quantified by ELISA.

Panels are representative of at least three different experiments. LE = long exposure, Supe = supernatant.

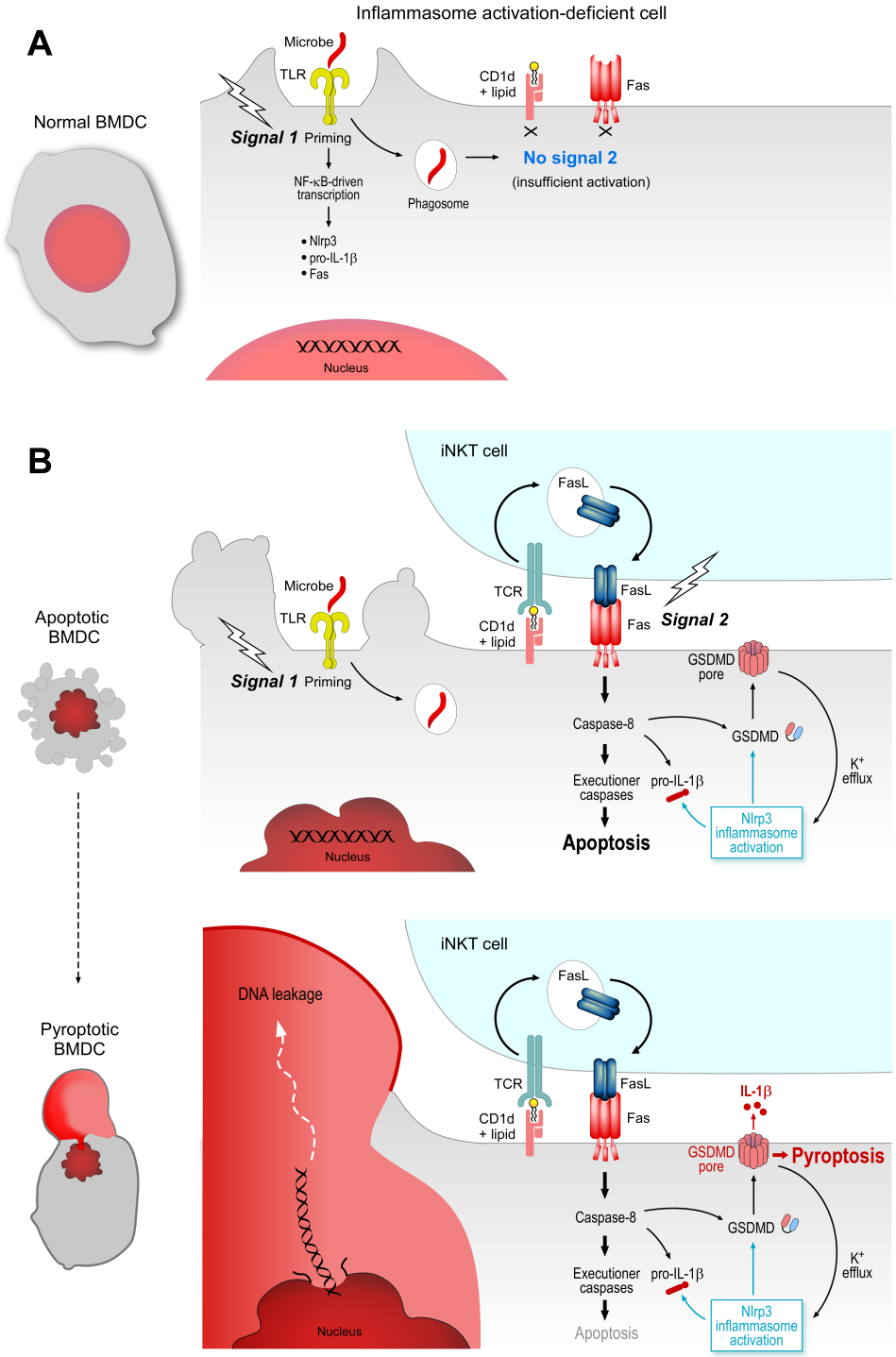

Figure S7 (related to figures 1, 2, 3, 4, 5, 6, and 7): Model for iNKT Cell-Induced IL-1β Release by TLR-Primed BMDCs

(A) Microorganisms that stimulate a TLR on a BMDC will provide it with an inflammasome priming signal, but they may fail to provide an inflammasome activating signal from within the cytosol of the host cell.

(B) BMDCs exposed to microbes can activate iNKT cells through the presentation of stimulatory self-lipid antigens on CD1d. In turn, the activated iNKT cell rapidly translocates intracellular FasL to the surface, ligates Fas on the BMDC, and activates a caspase-8-driven signaling module that initiates the apoptotic program and drives IL-1β processing and release in an inflammasome-dependent and -independent manner. Through caspase-8-mediated activation of the pore-forming activity of GSDMD, Fas ligation mediates potassium efflux, resulting in the activation of the Nlrp3 inflammasome. GSDMD mediates the switch from apoptosis to pyroptosis, resulting in the lytic, inflammatory death of the BMDCs characterized by the release of nuclear DNA into the cytoplasm and pyroptotic plasma membrane balloons. This two-cell model for IL-1β release can potentially trigger IL-1β release during infection with any microorganism that stimulates a TLR on the BMDC, even if the microbe fails to elicit cell-autonomous inflammasome activation.